Scheeres D. J., Britt D., Carry B., and Holsapple K. A. (2015) Asteroid interiors and morphology. In *Asteroids IV* (P. Michel et al., eds.), pp. 745–766. Univ. of Arizona, Tucson, DOI: 10.2458/azu_uapress_9780816532131-ch038.

Asteroid Interiors and Morphology

D. J. Scheeres
The University of Colorado Boulder

D. Britt
University of Central Florida

B. Carry
Institut de Mécanique Céleste et de Calcul des Éphémérides

K. A. Holsapple
University of Washington

The geophysical study of asteroids has moved from the realm of speculation and constraint to a more data rich environment where observations can be directly used to understand and probe the physical nature of these bodies. While many broad questions were posed in the *Asteroids III* chapter on asteroid interiors, in the current setting we are now able to probe more deeply into these questions, taking advantage of many different observations of asteroids across their entire size scale. The current chapter will take a very broad survey of what constraints currently exist in this area, what progress has been made in understanding these bodies analytically and through simulations, and what current theories can inform and guide future observations and tests of our understanding. The following topics are covered in this chapter: the strength of asteroid materials as inferred from meteors and meteorites, the density and porosity of asteroids as inferred from remote observations, global constraints on asteroid strength and morphology based on ground- and spacebased observations, analytical theories of asteroid strength and evolution, and the current state of numerical simulation techniques of asteroid interiors and morphology.

1. INTRODUCTION

The past decade has seen an astonishing array of advances across a wide spectrum of important inputs to the problem and mystery of asteroid interiors. These include the development of a large database concerning asteroid component strengths, as evidenced by meteors and meteorites (section 2); the compilation of extensive densities and inferred porosities for asteroids based on groundbased observations (section 3); the development of new computational techniques for the simulation of how asteroid rubble piles deform and fission or shed mass when subject to extreme rotation rates (section 4); and the development of crucial insights into the unique geophysics of specific asteroidal bodies (section 6). This chapter will review these different areas of advancements in an attempt to unify these disparate topics and show where future progress can be made in this field.

Knowledge about asteroid interiors is a crucial aspect for understanding these bodies, as it provides clues about their evolutionary history, in turn providing strong constraints on the history of the solar system. Unlike asteroid surfaces, it is impossible to peer directly within or easily take a sample measurement from within a body. Thus the study of asteroid interiors must rely on a combination of measurement and theory to develop constraints on the interior environment. Given these restrictions, previous investigations have studied observable characteristics that may be related to the nature of their interiors. This being said, there are measurement techniques that can probe the interior properties of bodies, in particular through seismic and radar sounding measurements. These are discussed in section 5 and represent a potential source for future advancements in this field.

The most accessible features of an asteroid that are related to their interior structure are the mass, density, shape, and spin. These are strongly constrained by the interior structure, and by the strength and mechanical properties of that structure. By focusing on these specific observables, we can start to answer basic questions about these bodies: How strong are they? What is the nature of that strength? Are the interiors rubble piles full of voids at various size scales, or are they solid coherent structures? How do these properties depend on composition, shape, spin, size, or location?

Important steps in answering the above questions have occurred since the publication of the *Asteroids III* volume

(e.g., *Asphaug et al.,* 2002; *Britt et al.,* 2002). These advances are related to the accumulation of fundamental data on these bodies through meteor falls and groundbased observations, analytical studies of the shapes of rubble piles, and ever more precise numerical simulations that probe the mechanics of rubble-pile interactions. We do note that our discussion will be more focused on the smaller asteroid bodies and rubble-pile structures, as this is where much of the progress has occurred in the last decade. This is not to discount the important results from the European Space Agency (ESA) Rosetta mission to asteroid (21) Lutetia or the NASA Dawn mission to asteroid (4) Vesta; however, we refer the interested reader to the chapters in this volume by Russell et al. and Barucci et al. for a detailed discussion of those scientific results.

The topic of asteroid interiors has been dealt with previously in the *Asteroids III* chapter by *Asphaug et al.* (2002). That chapter serves as a fundamental starting point for the current survey, and we assume that the interested reader is familiar with that work. The current chapter takes a different approach from that earlier work, reflecting the current thinking about what aspects of observations can be directly applied to understanding asteroid interiors. Another important resource from the *Asteroids III* book is the chapter on gravitational aggregates by *Richardson et al.* (2002). The current chapter extends that descriptive chapter in the direction of geophysics, striving to link the possible granular nature of asteroids with fundamental physical processes that occur for aggregates. The goal of that chapter was to distinguish the different ways in which a shattered body could exist, from a random assemblage to a coherent collection of components shattered in place from an initial monolithic body. The current chapter does not deal much with this distinction, although its implications do arise when discussing observations of macroporosity. What is new in the current chapter, with regard to gravitational aggregates, is the realization that such assemblages may have a small level of cohesion, which changes the dynamical evolution of these bodies in a significant and observable way. Additionally, not considered in that chapter was the size distribution of the particles of these aggregates, which has now been theorized to be a crucial aspect of their geophysics (*Sánchez and Scheeres,* 2014). Observations have not conclusively identified which of the many types of gravitational aggregates discussed in *Richardson et al.* (2002) might in fact exist in nature; however, many different observations (as discussed in this chapter) seem to fit best with their definition of "rubble pile," stated verbatim as: *"This structure is literally a pile of rubble, with the organization that you might expect from a bunch of rocks dumped from a truck. A body that has been completely shattered and reassembled may fit into this category."*

The outline of the chapter is as follows. In section 2 we focus on what we know about the fundamental strength and mechanical properties of the constituent pieces of asteroids as represented in the meteorite collection and meteor observations. From this study we find that there remain interesting and significant disconnects between the measured strength of meteorites and the inferred strength that they have based on the altitude at which they fail, which is expected to be related to their possible rubble-pile structure. This data provides insights into bodies up to several meters in size, but not beyond this limit.

In section 3 we use groundbased observations, and some spacecraft observations, to develop a wide range of constraints on how the constituent components of asteroids are assembled by computing their density and porosity. The implications are that some asteroids are highly porous bodies, in general, supporting the idea that these can be rubble piles. From this data there is also a clear progression of larger bodies having lower porosities, indicating the importance of gravitational compression. From this data we gain insight into the structure of bodies at the larger scale, ranging up to several hundreds of kilometers in size.

Section 4 applies and interprets the size-spin data for insight and motivation into an understanding of asteroid morphology and strength. From this data we can place constraints on the properties of the asteroid population and expose areas of uncertainty and ambiguity. Linking these observations with modeling and theories of asteroid strength has provided new insights and constraints on the global strength of asteroids, and provided clues as to their internal morphology. Theory and data from this section also help address the gap between the insights from meteorites on smaller bodies and from the groundbased studies of larger bodies.

Section 5 discusses the insights that can be inferred on asteroid interiors using the visible geology of asteroid surfaces, constraints on the transmission of seismic energy, and by an improved understanding of the rate of dissipation that may occur in asteroids. These methods indicate a potential pathway for better probing and determining the unique geophysical environment within small rubble-pile bodies.

Finally, section 6 focuses on a number of specific asteroids that have been observed with some level of precision since *Asteroids III,* with the exception of (4) Vesta. These include the targets of spacecraft missions, (433) Eros and (25143) Itokawa; the unique case of 2008 TC_3, which was analyzed both with groundbased observations and on the ground with meteorite falls; and a number of ground observed asteroids including (216) Kleopatra, (29075) 1950 DA, (66391) 1999 KW_4; and two active asteroids, P/2013 P5 and P/2013 R3. Many of these bodies are discussed in detail elsewhere in this book, but our discussions are focused specifically on what these bodies tell us about asteroid interiors and strength. Finally, overall conclusions are drawn and future areas where additional research and observations are needed are highlighted.

2. MATERIAL CONSTRAINTS

Meteorites and meteors are samples of materials from small bodies in near-Earth space, albeit transported from all regions of the solar system (see the chapter by Binzel et al. in this volume). Note that a meteorite and a meteor can be just different manifestations of the same object; a meteor is the visual and sonic phenomena of the small body transit-

ing Earth's atmosphere, while a meteorite is the surviving material that can be collected on the surface of Earth. As small bodies encounter Earth, their interaction with Earth's atmosphere, their mass loss on entry, the characteristics of their fall, and analysis of recovered fragments all provide clues about the structure, cohesion, and mineralogical homogeneity of the parent small bodies. This subsection is focused on summarizing and collecting in one place information on the strength of these bodies, both as individual components and as agglomerations when they first enter the atmosphere. For more information, see also the chapters by Borovička et al. and Jenniskens in this volume.

2.1. Meteorite Strength

An individual recovered meteorite is a direct sample of the material properties and strength of the components of small bodies. However, the samples that survive the stress of deceleration and atmospheric entry are necessarily biased toward the strongest and most coherent materials in the parent object. Weak and volatile-rich material tends to be destroyed on entry. Shown in Table 1 are the compressive strengths of a number of meteorites along with common materials for comparison [taken from *Popova et al.* (2011); see also *Kimberley and Ramesh* (2011) for additional data].

Natural materials can be very strong, such as individual crystals of quartz (1100 MPa). Single mineral strengths derive from the inherent strength of the crystal structure. Rocks are collections of minerals and their strength derives from a mixture of their mineral crystal strengths, their formation conditions, and the nature of the bonding between minerals. Igneous rocks like granite, for example (100–140 MPa), are composed of a substantial amount of quartz, but as a whole the bonding between their minerals makes the rock much less strong than the individual minerals. Unreinforced concrete at 20 MPa compressive strength is a good comparison standard.

Like rocks, there are substantial variations in the inherent strength of meteorites. Most ordinary chondrites (the most abundant type of meteorite fall) are much stronger than concrete. Volatile-rich carbonaceous chondrites are much weaker, and in some cases, e.g., the Tagish Lake meteorite (meteorites are named for the localities where they are recovered and in this chapter they will be often referred to by their meteorite name), their measured strengths are on the order of weakly consolidated soils (dirt clods).

Why are ordinary chondrites so strong? In general, they are conglomerates of chondrules (millimeter-sized spheres of minerals formed in the solar nebula), chondrule fragments, dusty matrix, and iron-nickel metal that have been welded together by varying levels of grain-boundary melting. In addition to welding in the silicates, the metal in ordinary chondrites provides a natural reinforcing mesh that is often interconnected in some ordinary chondrites that have been subjected to higher temperatures and thus have undergone some degree of remelting and metamorphic processing referred to as having higher metamorphic grades. As a result, high-metamorphic-grade ordinary chondrites can have many of the strength properties and reactions to stress of steel-reinforced concrete. However, there are some very weak ordinary chondrites. The Holbrook meteorite (Table 1) is a high-metamorphic-grade ordinary chondrite but is very weak and friable. Weston is also a high-grade chondrite but the individual chondrules are so poorly cemented that it falls apart with handling. The best analogy for this sample is a loosely glued collection of millimeter-sized spheres. However, the individual chondrules that are weakly held in Weston are individually quite strong.

The major exception to the story of relatively weak ordinary chondrite bolides is the large and well-studied Chelyabinsk

TABLE 1. Meteorite and material strength.

Material	Meteorite Type	Compressive Strength (MPa)	Tensile Strength (MPa)
Concrete — Unreinforced	Typical sidewalk	20	
Quartz	Single crystal	1100	55
Granite		100–140	
Medium dirt clod		0.2–0.4	
Holbrook, Arizona	L6 (OC)	6.2	
La Lande, New Mexico	L5 (OC)	373.4	
Tsarev	L5 (OC)	160–420	16–62
Covert	H5 (OC)	75.3	
Kunashak	L5 (OC)	265	49
Elenovka	L5 (OC)	20	2
Krymka	LL3 (OC)	160	22
Seminole	H4 (OC)	173	22.5
Plutusk	H5 (OC)	21.3	31
Hoba	Iron — ataxite	700	
Sikhote-Alin	Iron — octahedrite	410	44
Tagish Lake	C2 (CC)	0.25–1.2	
Murchison bolides	CM (CC)	~50	0.1–1

OC = ordinary chondrite; CC = carbonaceous chondrite. Data from *Popova et al*. (2011).

bolide and meteorite (*Borovička et al.,* 2013). While its first breakup was at high altitude (~45 km and 0.7 MPa), it underwent a series of fragmentation events. This included 11 fragmentations between 39 and 29 km under atmospheric dynamic pressure loads of 1–5 MPa and several boulders breaking off at 26–24 km under loads of 10–13 MPa. Interestingly, the main body remained relatively intact down to 22 km until its massive disaggregation at 18 MPa. This is probably due to the heterogeneities and highly shocked nature of the Chelyabinsk meteorite and the presence of extensive melt veins that welded portions of the meteorite.

Volatile-rich materials like the Tagish Lake meteorite are much different than the ordinary chondrite bolides. In this case the strength of the individual cobbles is roughly what is seen in the atmospheric breakup phenomena and this is the only case where the maximum compressive strength inferred in the atmosphere is greater than the compressive strength of the measured meteorite. This may be due to the presence of ice surviving in Tagish Lake. Recovered samples often expressed significant amounts of water when brought above freezing temperatures (*Brown et al.,* 2002), and samples of Tagish Lake that have been kept at freezing temperatures show lower porosity than samples that have been allowed to warm (*Ralchenko et al.,* 2014). It may be that ice-filled pore space within the meteorite provided extra strength for the bolide during atmospheric entry.

The meteorites listed in Table 1 are samples of hand- and cobble-sized survivors of atmospheric entry, which are the strongest and most coherent materials of the original small body. The vast majority of bolides do not survive entry as anything other than widely dispersed ablation dust. Typically the minority of small bodies that do survive entry lose approximately >95% of their preatmospheric mass (*Popova et al.,* 2011). Only a handful of bolides have been tracked to delivering material to the surface with that material recovered. Shown in Table 2 are bolides with recovered meteorites (*Popova et al.,* 2011).

TABLE 2. Select bolides with recovered meteorites (*Popova et al.,* 2011; *Borovička et al.,* 2013).

Meteorite (type)	Compressive Strength (MPa)		
	Range for Met. Type	First Breakup	Max.
Pribram (H5)	77–247	0.9	
Lost City (H5)	77–247	0.7	2.8
Innisfree (L5)	20–450	0.1	3
Chelyabinsk (LL5)	0.7	18	
Tagish Lake (C2)	0.25–1.2	0.3	2.2
Moravka (H5–6)	77–327	<0.9	5
Neuschwanstein (EL6)	3.6	9.6	
Park Forest (L5)	20–450	0.03	7
Villalbeto de la Pena (L6)	63–98	5.1	
Bunburra Rockhole (Ach)	0.1	0.9	
Almahata Sitta (Ure, OC)	0.2–0.3	1	
Jesenice (L6)	63–98	0.3	3.9
Grimsby (H4–6)	77–327	0.03	3.6

2.2. Bolides and Boulders

A bolide is roughly defined as a large, bright meteor that is typically brighter than the full Moon during its brief peak brightness. The physical phenomena are the result of a small body entering the atmosphere at hypersonic speeds [in the case of near-Earth asteroids (NEAs), velocities are in the range of ~12–20 km s^{-1}) and rapidly shedding their orbital kinetic energy into visible and thermal energy from friction with the atmosphere. As the body comes apart the initially compact mass fragments, exposing a larger surface area to rapid deceleration. This is seen as bright flashes within the bolide as smaller fragments rapidly heat, ablate, and decelerate. This typically occurs at altitudes ranging over 70–23 km and the small body's response to the atmospheric ram pressure can be used to estimate the body's coherent strength under compression (*Popova et al.,* 2011). These bolides are typically recorded on specialized optical tracking networks, but for the brightest objects security cameras and even dashcams are a valuable source of data (*Brown et al.,* 2002). Table 2 shows strength data from bolides with recovered meteorites. This permits a direct comparison of the strength of the surviving fragments with the strength estimated during the breakup of the small body on atmospheric entry.

Several points are readily apparent from Table 2. While most recovered meteorites are very strong, the initial breakup of the entering small body occurs at very low compressive stress. Initial breakup altitudes can be very high, as much as 70 km in some cases for the weakest bodies in Table 2, and the maximum compressive stress in Table 2 may occur at what are also substantial altitudes typically in the range of 35–20 km. For the initial breakup, these altitudes represent relatively low stresses, creating failures within weakly bound materials.

A question that has yet to be fully addressed is whether these stresses are consistent with some small asteroids being rubble piles, potentially held together by weak cohesive forces (see section 4.5). Examples of low-coherent-strength objects from Table 2 would include the Grimsby and Park Forest meteorites. However, while the first breakup provides insight into the strength of the entering body, the bolide phenomenon continues as the individual large pieces of the body break up under rising compressive stresses. Essentially these are the cobbles and boulders within the body shattering under rising stresses, and represent the state of fracturing and cohesion within individual components of the small body. For example, Park Forest started to fail under low compressive stress of 0.03 MPa, but the last major breakup was at more than 2 orders of magnitude greater stress. One possible explanation would be that the weak breakup occurred for a boulder within the rubble pile that failed along zones of preexisting weakness. While the basic material of ordinary chondrites is very strong, these objects are often pervasively fractured from a long impact and shock history and would be much weaker along their existing fractures. Indeed, that is the primary reason for multiple observations that large bodies are globally much weaker than smaller ones. However,

not all entering bolides fail under the stress of atmospheric entry. There are a number of examples of coherent "boulders" impacting the ground with little or no apparent fragmentation during entry. A recent example was the meter-sized boulder Carancas (H4–5) that created a 13-m-wide crater near Lake Titicaca in 2007 (*Borovička and Spurnỳ,* 2008).

2.3. Meteorite Showers

While coherent boulders occasionally do survive atmospheric entry, a much more typical case is the meteorite shower. These are small bodies that break up in the atmosphere similarly to the observed bolides. Table 3 includes a list of selected large meteorite falls (meteorites that were observed to fall from space) and finds (meteorites that were found some time after they fell). The discussion of atmospheric breakup and observed bolides has focused on stony meteorites, since so far no iron meteorite falls have been instrumentally recorded. On the other hand, irons are much stronger under compression and tension than stones and recovered irons are typically much larger than stones. Most of the recovered mass of meteorites are irons and the 15 largest meteorites are all irons. There are strong positive selection effects in finding irons since they are clearly unusual in the terrestrial environment. That said, note that of the largest irons, only two are single bodies. The largest meteorite in total mass is Campo del Cielo, which fell in at least 30 fragments. Most of the fragments are buried so the mass and fragment count is a rough estimate. The largest single body to reach the ground is either Hoba, which was found in a single mass, or Sikhote-Alin, which fragmented on impact (producing a 60-m-diameter crater and more than 9000 fragments).

For stony meteors, almost all the large mass meteorites are showers. Some of the more famous showers are listed in Table 3. With stones, the entry phenomena make it more likely that they will shatter in the atmosphere, producing a literal shower of rocky fragments. These fragments tend to be largely homogeneous. Investigations of several showers have, with one notable exception, not found significant mineralogical variation within the shower (*Consolmagno et al.,* 2008). The major exception is the Almahata Sitta fall, which was primarily ureilite material with a significant component of ordinary chondrite (see the chapter by Jenniskens in this volume). Heterogeneity within meteorites is not unknown and it is not uncommon to find xenoliths (different meteorite types, literally "foreign rock") incorporated into meteorite breccias (*Brearley and Jones,* 1998); however, the level of heterogeneity is typically pretty small. Xenoliths are usually confined to single or a few clasts within a much larger homogeneous matrix. The shower data suggests that an Almahata Sitta level of heterogeneity is rare. For discussion about Kaidun, see the chapter by Borovička et al. in this volume.

TABLE 3. Selected large meteorites and showers (*Grady,* 2000).

Meteorite	Date (dd/mm/yyyy)	Mass (kg)	No. Fragments
Campo del Cielo (IAB Iron)	Find	100,000	30
Sikhote-Alin (IIAB Iron)	12/02/1947	70,000	9000
Hoba (IVB Iron)	Find	60,000	1
Cape York (IIIAB Iron)	Find	58,000	8
Willamette (IIIAn Iron)	Find	14,500	1
Pultusk (H5)	30/01/1868	8863	70,000
Allende (CV3)	08/02/1969	5000	1000
Jilin City (H5)	08/03/1976	4000	100
Tsarev (L5)	06/12/1922	1132	40
Knyahinya (L5)	09/06/1866	500	1000
Mocs (L6)	03/02/1882	300	3000
Homestead (L5)	12/02/1875	230	
Holbrook (L/LL6)	09/06/1866	218	14,000
Forest City (H5)	02/05/1890	122	2000

2.4. Summative Discussion

The data presented here on meteorites, bolides, and showers provides some basic insights on the structure of meteorite parent bodies up to several meters in size. For stony bodies of even a few meters in diameter, rubble piles seem to be the norm. The relatively low stresses on breakup seen in most of the bolides and the prevalence of showers for large stones point to a rubble-pile structure being very common. The individual components of these aggregates can be very strong, ranging up to an order of magnitude stronger than concrete, but the overall body is very weak. Volatile-rich bodies are both individually and collectively very weak.

Mineralogical homogeneity seems to be the general rule in small bodies. While there are significant exceptions and xenoliths are not uncommon, the shower data point to largely homogenous small bodies. Finally, for small bodies, irons are easily the strongest and most-coherent materials. Their large compressive and tensile strengths and apparent relatively low fracturing result in irons being by far the largest meteorites that survive atmospheric entry. However, they are relatively rare in the fall population, and the selection effects of their large strength suggest they are overrepresented in the fall population relative to their share of the NEA population.

3. ASTEROID BULK PROPERTIES

The next section probes the interiors of asteroids through a different approach, based on determining their bulk densities and bulk porosities. This takes us beyond the strength of the individual components of asteroidal bodies, either determined by measurements on meteorite falls or through inferred strengths in the upper atmosphere. The bulk densities are found by comparing mass estimates to volume or size estimates for these bodies. Bulk porosities are estimated by comparing the bulk densities to the asteroid spectral type, to determine likely grain densities and hence bulk porosities

The fundamental data compiled here concerning asteroid densities and macroporosities are presented in Figs. 1 and 2. Details on how the data were compiled are given in *Carry* (2012), and are not repeated here. While the previous section

was focused on meter-sized bodies, the focus in this section is necessarily on the other end of the scale, with most of the reliable data on densities and porosity existing for larger bodies, up to hundreds of kilometers. Only in a few situations are there good data on smaller bodies.

The first evidence on asteroid interiors was derived from meteorites, with identification of differentiated and nondifferentiated internal structures (see section 2). Dynamical families, originating from catastrophic disruptive collisions, provide another way to study asteroid interiors. Clumps of asteroids identified dynamically (e.g., *Bendjoya and Zappalà,* 2002) also share common surface properties, which are in turn used to discriminate genuine family members from the background population (*Parker et al.,* 2008; *Carruba*

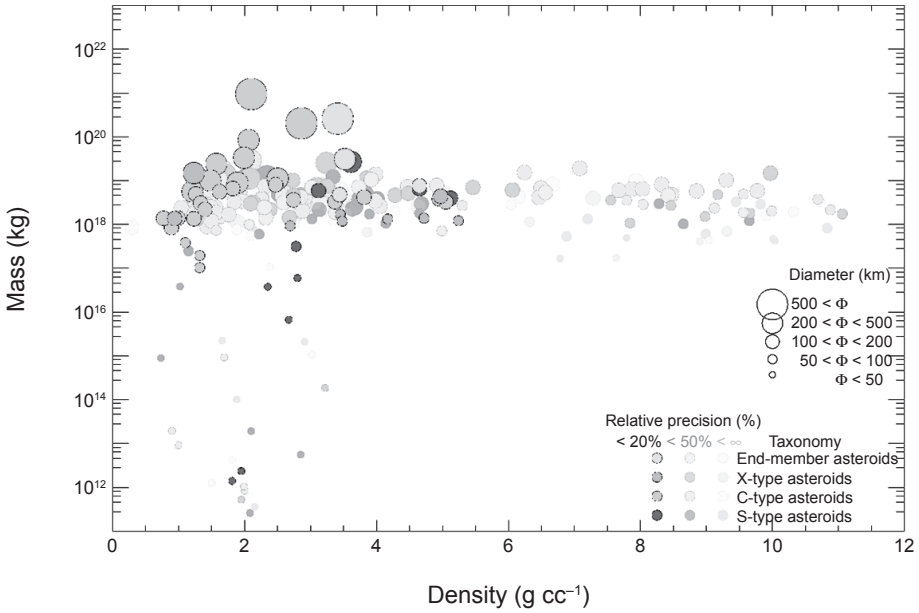

Fig. 1. See Plate 24 for color version. Density vs. mass. Asteroids are divided into four taxonomic groups (from *DeMeo et al.,* 2009): S-complex in red, C-complex in gray, X-complex in green, and end members in yellow. The size of the symbols indicates the asteroid diameter, below 50 km, between 50 and 100 km, 100 and 200 km, 200 and 500 km, and above 500 km. The three different levels of contrast correspond to three cuts of relative accuracy: <20%, <50%, and regardless of precision (<∞).

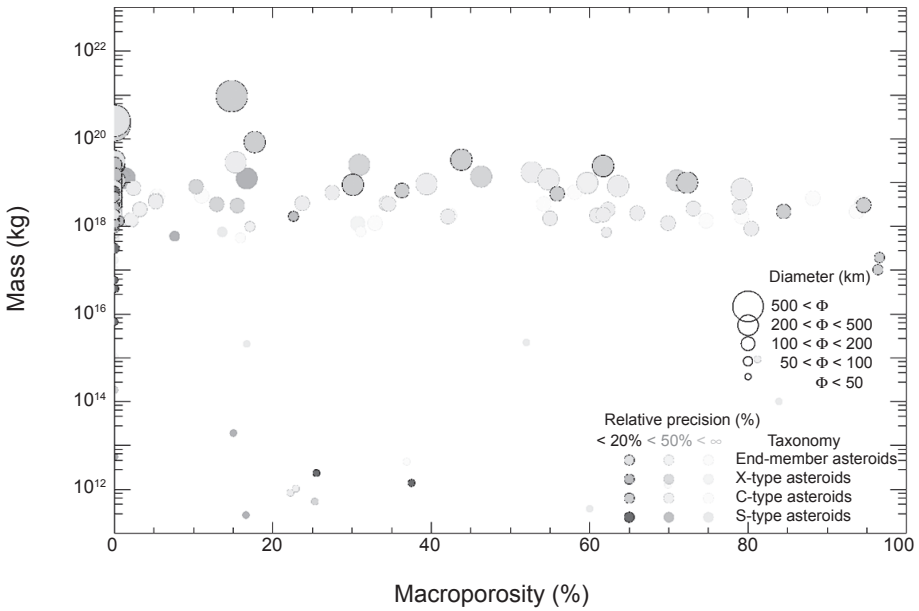

Fig. 2. See Plate 25 for color version. Macroporosity vs. mass. See Fig. 1 for the explanation of symbols.

et al., 2013). Such similarities are suggestive of a homogeneous interior for the parent bodies of these families (see the chapter by Michel et al. in this volume).

3.1. Density

Density is perhaps the most fundamental property for discriminating the composition and internal structure of asteroids (*Britt et al.,* 2002). It is also extremely difficult to measure, and the number of precisely measured asteroid densities is still very limited. This is because both mass and volume are required to determine the density of an asteroid.

Estimating any mass at all is a challenge, owing to the relatively low mass of asteroids as compared to other planetary objects. The exception is for binary asteroids, for which the total mass can be easily estimate (see the chapter by Margot et al. in this volume). The number of mass determinations thus limits the number of density estimates. The precision of these estimates is, however, limited by the uncertainty on asteroid diameters (*Carry,* 2012).

Any determination of the mass relies on measurements of the gravitational interaction between the target asteroids and other objects. The most accurate estimates (at a few percent accuracy) are derived from radio science experiments during spacecraft encounters [orbit or flyby (e.g., *Yeomans et al.,* 2000; *Abe et al.,* 2006; *Pätzold et al.,* 2011)] and studies of binary asteroids (see the chapter by Margot et al.). The vast majority of asteroids, however, have never been visited by spacecraft nor possess satellites [only a handful of large asteroids possess satellites, albeit the fraction is higher at smaller size; about 15% of near- Earth asteroids have satellites (*Margot et al.,* 2002)]. It is nevertheless possible to determine their mass from the gravitational pull they exert on other planetary objects: asteroids, planets and their satellites, and interplanetary spacecrafts (see, e.g., *Hilton,* 2002; *Fienga et al.,* 2008; *Kuchynka and Folkner,* 2013; *Goffin,* 2014).

Methods based on long-range influence rely heavily on the modeling of all relevant gravitational effects and interactions in the solar system (e.g., asteroid ephemerides, planets, general relativity) and are therefore more prone to systematic errors, and current precision is still limited to date [often above 50%, see the dispersion of estimates, together with the discussion on the accuracy and biases affecting mass estimates, in *Carry* (2012)]. Current samples of asteroid masses are therefore strongly biased. First, the best determinations are for binaries, but there may be differences between binary and single asteroid internal structures and thus extrapolating the density determined from binary asteroids to the whole population may introduce biases. Second, only large asteroids are massive enough to perturb the orbits of other objects. Thus this sample is mainly limited to asteroids larger than 100 km, while there is evidence for a size-dependence of the density owing to a different level of macroporosity [see Fig. 2 below and Fig. 9 in *Carry* (2012)].

The situation for diameter estimates is less dramatic. There are many techniques to measure the apparent size or surface area of an asteroid, and diameter estimates are available for tens of thousands of objects (e.g., *Masiero et al.,* 2011). Although diameter estimates are less prone to systematics than mass estimates [values generally agree to within measurement uncertainties (see *Carry,* 2012)], their contribution to the density uncertainty overwhelms that of mass. Diameter determinations have to be as accurate as 2–3% to allow density estimates to be more precise than 20%, a level over which density estimates hardly provide constraints. While simple modeling can have systematics above this level, realistic descriptions of asteroids, including knowledge of spin and three-dimensional shape, can provide this level of accuracy (see the chapter by Durech et al. in this volume).

Despite these limitations, the field of asteroid density has seen a revolution since the time of *Asteroids III* (*Britt et al.,* 2002). There has been a tenfold improvement in sample numbers (from 20 to 320), spanning many different taxonomic classes (and hence composition), diameters, and heliocentric distance (*Carry,* 2012). The upcoming decade will certainly provide many more determinations with a high level of accuracy. First, the stellar catalog at the microarcsecond level provided by the ESA Gaia mission should improve the precision on asteroid astrometry by an order of magnitude. Mass determinations from orbital perturbations should therefore become more precise. The observation of asteroids by Gaia will also allow the determination of the mass of about 150 asteroids with a relative precision better than 50%. It is even expected that 50 of these determinations will be more precise than 10% (*Mouret et al.,* 2007). The number of known binaries is also constantly increasing, adding to the number of high accuracy density estimates (see the chapter by Margot et al.).

3.2. Macroporosity

A density estimate by itself can restrict the list of possible components of an asteroid's composition. For example, a low-density asteroid such as (617) Patroclus [$\rho \approx 1$ g cm^{-3} (*Marchis et al.,* 2006; *Mueller et al.,* 2010)] cannot host large fractions of dense material or even silicates. The internal structure can be constrained using a comparison of the asteroid bulk density (ρ_A) with the grain density of its most likely constituents (ρ_C), as determined from study of the surface composition (see the chapter by Reddy et al. in this volume).

If $\rho_A \ll \rho_C$, the asteroid is underdense. This points toward large-scale voids or the presence of low-density material (i.e., volatiles) in its interior. While this is a typical case for comets, many asteroids are also seen to have porous internal structure. The porosity p, i.e., the fraction of volume occupied by empty space ($p = 1–\rho_A/\rho_C$), provides a measure of these structures. Because meteorites have microporosity (empty spaces at the grain-size scale, noted p_m), the macroporosity $\mathcal{P}$ has been defined as the fraction of volume occupied by large voids, i.e., $\mathcal{P} = p–p_m$. The question of the distribution of these volatiles or voids inside the asteroid remains open (*Britt et al.,* 2002). Following the terminology of *Richardson et al.* (2002), we can ask whether they are the results of cracks within a shattered monolith,

or interstices of a rubble pile formed through gravitational reagglomeration after a disruptive collision.

If $\rho_A \gg \rho_C$, the asteroid is overdense, and some high-density material must be present in its interior. This could be due to gravitational self-compression, differentiation (e.g., *Russell et al.,* 2012), or the result of the collision between two bodies of different densities. Most asteroids with a mass above 10^{19} kg are overdense, while the majority of asteroids below that threshold present some level of macroporosity. This is consistent with large bodies having enough internal energy from accretion and radioactive decay to differentiate.

If $\rho_A \approx \rho_C$, no clear conclusions can be made. However, given the comparable spectral properties observed among members of dynamical families, it may be reasonable to assume that the body is homogeneous.

3.3. What Can Be Concluded

Based on the data presented in Table 4 and Figs. 1 and 2, and more fully discussed in *Carry* (2012), there are a number of overall conclusions that can be drawn from these compilations, listed below.

- Asteroids in the S-complex are on average more dense than those in the C-complex.
- Asteroids in the C-complex seem to have larger macroporosity than those in the S-complex, hinting at a looser structure.
- The density of asteroids from both the S-complex and the C-complex seems to increase with the mass, apparently resulting from a decreasing macroporosity.
- In both the C and S-complex, NEAs (with masses from 10^{11} to 10^{16} kg) seem to have a lower density than main-belt asteroids, following the trend between mass and density observed for large asteroids.
- At comparable sizes, B-types appear significantly denser ($\rho \sim 2.4$ g cm^{-3}) than the other types of the C-complex that gather around $\rho \sim 1.4$ g cm^{-3}.
- While asteroids in both C- and S-complexes have narrow density ranges (with a few exceptions), asteroids in the X-complex covers a larger range, from the most dense Xc-types with $\rho \sim 4.9$ g cm^{-3} to X-types with $\rho \sim 1.8$ g cm^{-3}.
- Dwarf-planets (with masses above 10^{20} kg) apparently have little macroporosity, contrary to small bodies whose masses are inferior to $\approx 10^{20}$ kg (*Consolmagno et al.,* 2008).
- With the exception of NEAs, the dispersion in density and macroporosity is huge.

3.4. Future Prospects

As discussed above, the accuracy and reliability of density estimates have seen dramatic improvement since the time of *Asteroids III*. Even though many estimates still suffer from mild inaccuracy, the techniques are constantly being refined, and the next decade will provide more, increasingly reliable density measurements. A major issue still to be resolved is, how certain are the link between asteroids and meteorites? Based on their spectral properties, asteroids are classed within taxonomies (e.g., *Tholen and Barucci,* 1989; *Tedesco et al.,* 1989; *Bus and Binzel,* 2002). The latest to date by *DeMeo et al.* (2009) defines 26 classes, but analog minerals and meteorites have been identified for only 50% of them (see the chapters in this volume by DeMeo et al. and Reddy et al.). In other words, we have no reference density for half the taxonomic classes among asteroids. Discovering this meteorite-asteroid link is crucial for future interpretations of asteroid interiors.

4. ASTEROID STRENGTH AND FAILURE LIMITS

In addition to the constraints on asteroid density and porosity that can be determined from the population of ob-

TABLE 4. Average density, porosity, and macroporosity for the 12 (out of 26) taxonomic classes where density determinations more accurate than 20% are available ($\mathcal{N}$ determinations).

Class	Met.	$\mathcal{N}$	Density (g cm^{-3})	Porosity (%)	Macroporosity (%)
S	OC	11	2.72 ± 0.54	30.88 ± 8.76	25.28 ± 31.67
Sq	OC	2	3.43 ± 0.20	3.79 ± 0.35	–1.81 ± 2.16
B	CV	2	2.38 ± 0.45	38.66 ± 10.63	16.86 ± 6.81
C	CI	5	1.33 ± 0.58	84.96 ± 52.43	49.96 ± 43.61
Cb	CI	3	1.25 ± 0.21	96.80 ± 23.11	61.80 ± 20.86
Ch	CI	9	1.41 ± 0.29	74.47 ± 21.73	39.47 ± 16.29
X	EL	8	1.85 ± 0.81	90.81 ± 56.70	86.91 ± 147.58
Xc	Mes	2	4.86 ± 0.81	–9.47 ± 2.49	–14.47 ± 28.74
Xe	EH	1	2.60 ± 0.20	40.00 ± 4.42	36.20 ± 47.49
Xk	Mes	3	4.22 ± 0.65	4.27 ± 1.05	–0.73 ± 1.46
K	CV	1	3.54 ± 0.21	–6.78 ± 0.72	–28.58 ± 5.31
V	HED	3	1.93 ± 1.07	68.39 ± 53.72	57.39 ± 71.55

The analog meteorite of each class is listed. A negative porosity is indicative of an "overdense" structure. Table adapted from *Carry* (2012).

served asteroids, there are also significant constraints that can been gleaned from the combined data on asteroid spin rates, spin states, morphology, and sizes, filling the gap between meter-sized meteors (section 2) and kilometer-sized asteroids (section 3). The significant data for these inferences are summarized in Fig. 3, which shows asteroid diameters and spin rates taken from the database described by *Warner et al.* (2009). Also indicated on this figure are those asteroids that are tumbling or are binary asteroids, and a number of spin-limit curves as a function of different cohesive strength theories (all to be discussed later). Over the last few decades these observations have accumulated to the point where useful inferences on asteroid morphology can be made. In Fig. 3 we only show those bodies that have a quality measure of 2⁻ or higher, meaning that these observations are deemed reliable. It is interesting to note that there are a number of unconfirmed observations of spin periods (i.e., of quality measured less than 2⁻ and thus not shown in the figure) that could be significant if shown to be true. These are discussed later, in the hopes of motivating additional observations.

This data has motivated several different theories for the strength and morphology of asteroids. Significant among these is a better understanding that the spin limits do not require the rubble-pile hypothesis for almost all asteroids, the cohesion hypothesis in rubble-pile bodies, and the existence of tidal dissipations within such bodies. In the following subsections we discuss these issues in more detail, trying to integrate the physical and mathematical theories used to explain certain aspects of this data alongside a discussion of the data itself.

The precursor to these studies was given almost 20 years ago by *Harris* (1996), in which he noted that no asteroid had a spin period shorter than about 2.2 h and that the spin periods of objects in a given size range abruptly truncate at that value. He noted that this limit is essentially the spin rate $\omega_s = \sqrt{4\pi G\rho/3}$, where G is the gravitational constant and $\rho \sim 2.2$ is the bulk density, at which internal tensile stresses would be present within a spherical, constant density object (the actual spin rate for a body also depends strongly on its elongation). This spin rate also corresponds to local circular speed at the surface of the body, at which centrifugal forces equal the gravitational attraction of the body. From that connection he concluded that all or most asteroids must have a rubble-pile structure, as defined earlier, although that is not

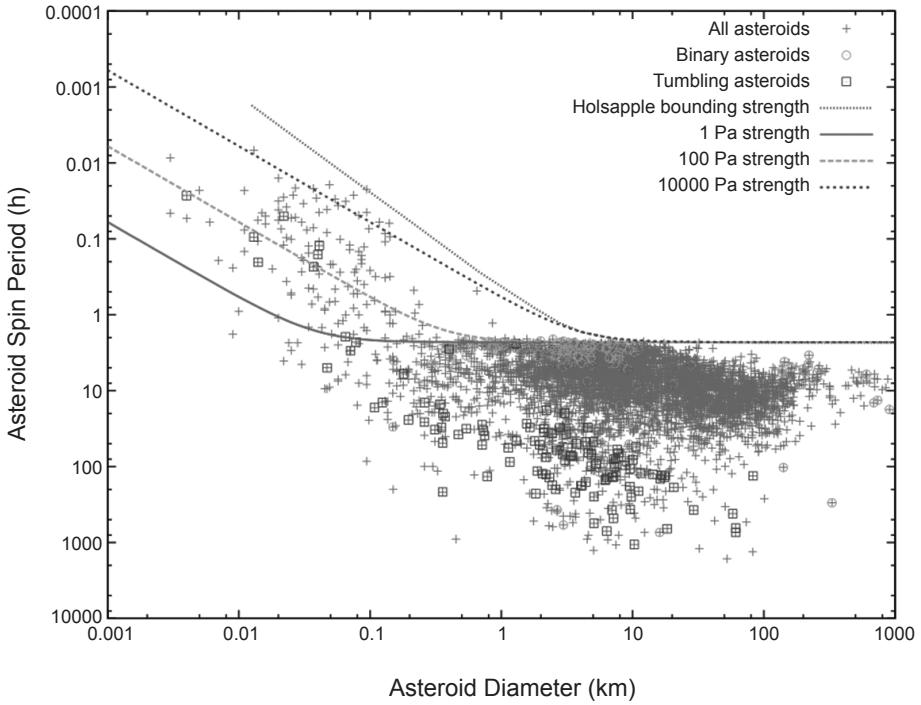

Fig. 3. See Plate 26 for color version. Asteroid size vs. spin period, with binaries and tumblers called out specifically. All others are assumed to be single, uniform rotators. Only bodies with periods deemed to be reliable (see *Warner et al.,* 2009) are shown. The plot shows distinct structures. No object larger than a kilometer in diameter spins faster than an ~2.4-h period, now known as the gravity spin barrier and that is understood to not be an indicator of cohesionless material by itself. Instead it is simply that at these size scales the gravity effects dominate any strength effect. A number of smaller bodies spin faster; those must experience tensile stress and must have some cohesive strength to hold together. Typically, the observed maximum spins are larger for smaller sizes. Also plotted are spin limits as a function of diameter for levels of asteroid strength. Data shown is as of August 2014.

the current interpretation. In addition, he also predicted that asteroids could spin faster than this limit if they had some strength, although no such asteroids were known at that time. He suggested there would be two regimes for spin, a gravity-dominated regime for larger asteroids and a strength-dominated regime for smaller asteroids. He suggested that in the strength regime their spin could increase inversely proportional to the diameter of the object. Since that paper, these ideas have been essentially verified and expanded, but with clarifications and new interpretations. A number of "fast spinners" have been found with shorter periods; however, they are all less than 1 km in diameter. And there have been detailed modeling studies deriving the relation between asteroid shape, maximum spin, and internal properties.

4.1. Analytical and Numerical Models of Rubble Piles

We first provide a brief review of current and past methods used to model asteroids, their interiors, and their morphologies. Studies of relations between shape, density, and spin of isolated self-gravitational bodies dates back several centuries, but mainly in application to fluid bodies. In those cases, the nature of the bodies was assumed to be fluid, the spin was known, and the goal was to determine the permissible shape. In 1687, Isaac Newton determined that the shape of a fluid Earth with gravitational and rotational forces is a slightly oblate spheroid. In 1742, Colin Maclaurin extended the work to discover the existence of equilibrium oblate spheroidal shapes with large ellipticity for rotating bodies with self-gravity, now called the "Maclaurin spheroids." *Jacobi* (1834) discovered the "Jacobi ellipsoids": equilibrium ellipsoidal shapes with three unequal axes. *Roche* (1850) added tidal forces during an orbit around a parent body and determined that there is a limit to the orbit radius, the famous Roche limit, inside of which there are no equilibrium solutions. *Poincaré* (1885) discovered other pear-shaped, non-ellipsoidal possibilities for equilibrium. *Chandrasekhar* (1969) gives a complete exposition of these classical works. A number of authors have used those fluid limits to infer limits on the mass density or density distribution of solar system bodies, although the mass density dependence can be swamped by other factors, the most important of which is the nonfluid composition. A separate approach to analyzing the internal stress properties of a nonfluid gravitating ellipsoid was given by *Chree* (1895), using linear elastic response from an initial stress-free state to model the mechanics of a self-gravitating body. This approach has motivated some modern study as well, discussed later.

Just as for a fluid, an ideal rubble-pile body can be assumed to have no tensile strength. But that does not mean that it behaves as a fluid. Consider an idealized rubble-pile body consisting of dry sand. Sand is an assemblage of relatively rigid, angular, submillimeter-sized grains that must interact during deformations. In a shearing deformation, the grains must move up and over adjacent grains. That motion is suppressed if the sand is subjected to a compressive pressure such as from gravity. That simple physical idea is the basis for the standard continuum soil mechanics models of failure, the Mohr-Coulomb and the Drucker-Prager criteria. In those models, the shearing strength is strongly increased by a compressive pressure in a relation that is assumed to be linear. The coefficient of that linear form is called the "angle of friction," although its presence is due to the interlocking of grains, not surface friction. These criterion have similar results, although Mohr-Coulomb is considered to be more accurate while Drucker-Prager is easier to handle analytically. It is the basis for the important difference between the behavior of water and the behavior of sand. The shearing resistance of water is independent of the confining pressure so that the angle of friction is zero. From this example it is clear that a material with no tensile strength can certainly have other strengths, including shear strength.

For that reason, the classical fluid theories relating shape and spin do not apply to rubble-pile, asteroid objects. *Holsapple* (2001, 2004) presented a comprehensive study of the relations between shape, spin, and internal properties for rubble-pile objects as a direct generalization of the historical fluid theories, and includes them as special cases. He assumed constant mass density, a general ellipsoidal shape, and in *Holsapple* (2001) a Mohr-Coulomb and in *Holsapple* (2004) a Drucker-Prager failure model. He was able to derive specific algebraic relations for the maximum spin allowable as a function of internal density, ellipsoidal shape, and angle of friction. *Sharma et al.* (2009) and *Sharma* (2013) analyze the problem following a somewhat different methodology and find similar results. Other studies on the stability of a continuum model of asteroids have also been made more in line with the classical approach developed by *Chree* (1895). In particular, *Dobrovolskis* (1982) studied internal stresses in Phobos; *Washabaugh and Scheeres* (2002) study the energetics of nonfluid, self-gravitating ellipsoids using a linear elastic model with a Young's modulus and Poisson ratio; and *Kadish et al.* (2005, 2008) studied stresses in bodies grown by accretion.

In the analytical realm Scheeres has also pursued the understanding of how a collection of self-gravitating rigid bodies evolves when subject to increasing spin rates. These studies have mainly focused on the dynamical stability of fissioned bodies (*Scheeres,* 2002a, 2009b), conditions for when bodies will transition from resting to orbiting configurations (*Scheeres,* 2002b, 2009a), and identification of different possible resting states that bodies may have when in contact (*Scheeres,* 2002b, 2012). These analyses are, by default, somewhat simple, although there are a few general results that can be discerned.

Over this same time period a number of researchers have pursued the modeling of cohesionless asteroid rubble piles using numerical methods, primarily with discrete element method (DEM)-based approaches. There have been two major modeling directions that have been used, the so-called hard-sphere DEM (HSDEM) and soft-sphere DEM (SSDEM) models. An HSDEM code models all particle interactions as impulsive, and thus does not directly determine or track forces. This is a computational simplification that allows for relatively rapid combined dynamical and interaction

computations, but makes it difficult to track or determine interior stress states or conditions. An SSDEM code allows for particle deformation (using an analytical model), and thus directly computes contact forces between the grains. This provides a more natural and realistic way for computing rubble piles in a condensed phase, as the grains are then allowed to come to complete rest with each other (which is impossible in an HSDEM as it only models two-body interactions), form force chains, and enable the internal stress state of the modeled body to be computed. The chapter by Murdoch et al. in this volume provides a more detailed discussion of HSDEM and SSDEM codes as applied to asteroids.

Some representative initial studies in this area for modeling asteroids were done by Richardson's group using an HSDEM code (*Richardson et al.,* 1998, 2005; *Walsh and Richardson,* 2006). They studied the ability of a collection of same-sized grains with a given level of spin to form a stable configuration, with the use of classical Jacobi or Maclaurin ellipsoids used as a measure of stability, and explored how such bodies would deform and fission following a planetary flyby or when subject to a rapid rotation rate. The mechanical properties of the grains are not directly controlled in these studies; in particular, the friction angle is simulated by having the grains either fall into a crystalline-packed matrix or through the use of a bimodal grain size distribution to promote a loss of friction (*Walsh et al.,* 2012).

Sánchez and Scheeres introduced a self-gravitating SSDEM model for describing the global behavior of rubble-pile bodies (*Sánchez and Scheeres,* 2011, 2012), in part to overcome such limitations. These models used grains with a size dispersion to avoid crystallization. The friction angle of the rubble pile is controlled by surface friction and interlocking. With this approach it becomes possible to track the internal stress and failure conditions using a granular mechanics code. Relevant results are given below.

An additional approach to the modeling of asteroid rubble piles was introduced in *Hirabayashi and Scheeres* (2014) and applied in *Hirabayashi* (2014) and *Hirabayashi and Scheeres* (2015). In this approach a detailed asteroid shape model can be used and the interior stress states computed by using commercial finite-element-analysis methods. This approach has the significant capability of being able to develop detailed models for the failure of asteroids when subject to gravitational and inertial forces. The use of a general approach enables the detailed analysis of plastic deformation modes and inclusion of detailed continuum model parameters such as Poisson ratio, cohesion, and angle of friction.

4.2. Rubble-Pile Shapes

Using the methods outlined above, the most fundamental question to be asked is what the expected shape of a rubble pile should be. Some insight can be gained by observing the surface slopes of asteroids, as these can indicate if there are regions that are clearly beyond the angle of repose for geological granular material; however, this cannot always be clearly linked to the internal processes. A number of different asteroid slopes have been computed in the past for specific shapes, and a recent analysis by *Richardson and Bowling* (2014) shows that most asteroids with known shapes have the majority of their surfaces beneath a typical angle of repose for granular material of ~35°. While there are some specific bodies that have significant regions of their surface that are clearly beyond these angles, such as (6489) Golevka (*Hudson et al.,* 2000) and (4179) Toutatis (*Hudson et al.,* 2003), such situations have not been commonly found in the estimated asteroid shapes described to date.

There have been some attempts at approaching the stability of rubble-pile asteroids through analysis of their shapes alone. *Harris et al.* (2009) and *Minton* (2008) approached the problem by analyzing the expected shapes of an asteroid where the surface slopes are constrained to be less than or equal to a certain limit. These analyses were used to explore the likely surface environment of rotationally symmetric, spheroidal asteroids commonly found to be the primaries of binary systems. The poster child of such asteroid shapes is (66391) 1999 KW_4–Alpha, which exhibits many peculiar features that are indicative of this body to be at or near its failure limit. More recently, *Scheeres* (2015) has studied these bodies using an approach that is fundamentally motivated by the surface slopes and combines some of the methodology from *Harris et al.* (2009) along with orbital dynamics considerations.

Such analyses are limited, however, in that they do not consider the totality of the mechanical principles that must be accommodated in order to say with certainty whether a given shape is stable or not. Indeed, it is possible for a given shape to have low slopes across its surface (even zero slope, and much less than the angle of repose), yet be structurally unstable as viewed from a mechanics point of view, which also considers its internal stress field and common failure theories. The necessary approach for that sort of analysis requires the development of a stress field within the body that accounts for all internal forces and that vanishes at the surface. The development of such stress fields is not in general unique. However, if one assumes linear elasticity, an ideal ellipsoidal shape, and a stress-free initial state, then a unique stress field can be derived. Given such a stress field, it is then possible to evaluate it against a failure theory, with the most commonly used ones being the Mohr-Coulomb or Drucker-Prager theory. For a cohesionless body these are simply specified as a function of their interior stress field for a given internal friction angle. Furthermore, there is only one stress state that is in equilibrium and also at the failure limit at each interior point. That occurs at a higher spin than for the elastic solutions, and provides the maximum possible spins among all possible stress fields.

In a series of papers, *Holsapple* (2001, 2004) applied this basic approach and evaluated the limit spins as a function of the ellipsoidal shape of a large range of asteroids modeled as ellipsoids of axes $a \geq b \geq c$. A representative result is given in Fig. 4, which depicts the maximum equilibrium spin as a function of the aspect ratio b/a, for a prolate object ($a > b = c$), along with data for a number of asteroids. The limit

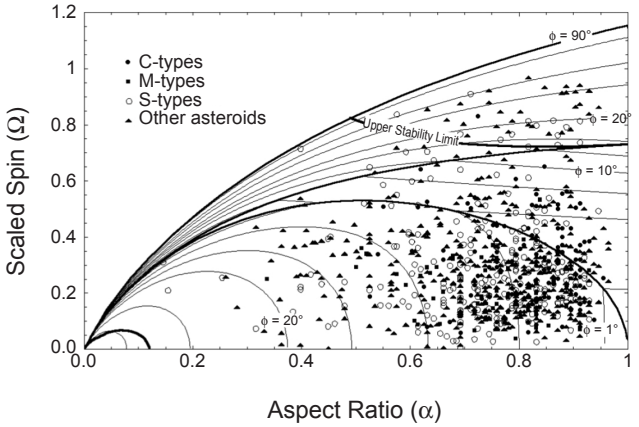

Fig. 4. Maximum equilibrium spin limits (Ω) for a prolate rubble pile body as a function of its aspect ratio defined as its polar extent over its total length, (α = c/a). The spin limit is normalized to be independent of density and depends upon the angle of friction, (ϕ), and for each angle of friction there is an upper spin limit and a lower spin limit. At the upper limit equilibrium cannot be achieved for a larger spin and at the lower limit equilibrium cannot be achieved for a smaller spin. Under the dictates of the theory all the asteroid objects plotted, even if not exactly ellipsodidal, must have some nonzero angle of friction arising from a particulate structure. See *Holsapple* (2001) for a more complete discussion of this figure.

spin is found to depend explicitly on the angle of friction, as is shown in the curves, which for most soils is on the order of 35°. (A fluid body with spin cannot be exactly prolate, but instead must have a Jacobi shape. Therefore it does not appear on this figure.)

Spherical asteroids are represented at the right abscissa of Fig. 4. As an example computation, assume a 35° angle of friction and a mass density of 2.5 g cm^{-3}. From this analysis the body cannot have a period shorter than 2.5 h before it begins to deform. However, the period at which a loose surface particle would spin off that spherical object is $p_s = 2\pi = (\omega_s 3600) = 2.08$ h, the case noted by Harris (note that the surface speed for escape from a spherical asteroid is a factor of $\sqrt{2}$ faster than the spin-off speed, so a particle would not escape after spin-off unless the spin period was shorter than 1.5 hr). Between these limits loose particles spun off could remain around the asteroid for some period of time. A similar elongated ellipsoidal object with an aspect ratio of 0.5 has a deformation spin period limit of 4.2 h and the particle spin-off limit of 2.9 h.

These theoretical results add detail to the basic idea that rubble-pile asteroids cannot spin faster than some well-defined limit, with specific results about the dependence of that limit spin on the actual shape, density, and internal strength of an object. For the idealized ellipsoidal case, elongation lowers the spin limit, but not as much as the linear decrease as suggested in *Harris* (1996).

On a case-by-case basis these analyses can be compared to calculations with numerical codes. A particle-based analysis of equilibrium shape was presented by *Richardson et al.* (2005) using an HSDEM code with 1000 total particles. They considered a spinup of an initial shape and the subsequent reformation to an equilibrium shape. Those reformed equilibrium shapes were roughly consistent with the Holsapple continuum limits discussed above, but for an angle of friction of ~40°. Subsequent analysis by *Walsh et al.* (2012) indicated that the effective friction angle of their stacked hard-spheres was on the order of 40°, leading to consistency with this result. It is also relevant to note that *Washabaugh and Scheeres* (2002) showed that the total energy of ellipsoidal shapes at a given level of angular momentum was minimized in a broad region in the vicinity of the Jacobi and Maclaurin ellipsoids. While not providing specific failure conditions, their analysis did include the effect of Poisson's ratio in their stress field, accounting for a non-incompressible condition that has been associated with granular materials. In another study, *Tanga et al.* (2009) demonstrate the ability of rubble piles modeled with HSDEM to evolve toward the fluid equilibrium shapes of Jacobi and Maclaurin ellipsoids when subject to intermittent "shaking" due to relatively small impacts.

4.3. Deformation of Rubble Piles

A natural follow-on question regards the expected shape deviation of a rubble-pile body when subject to a changing angular momentum. For asteroids such changes in angular momentum are known to occur for smaller bodies due to the Yarkovsky-O'Keefe-Radzievskii-Paddack (YORP) effect (see the chapter by Vokrouhlický et al. in this volume) and for larger bodies due to impacts. The outcomes of such evolutionary questions can only be addressed through theory and simulation; however, such studies are important as they provide predictions for what may occur in actual asteroid systems.

This question of the fate of an object as its spin limit is slowly subjected to additional angular momentum was analyzed using a continuum model in *Holsapple* (2010). Such an object must globally change shape once it reaches the limiting failure condition outlined above in order to remain stable. Holsapple assumed that the body transitions through a sequence of evolving ellipsoidal shapes. The dynamical theory leads to an ordinary differential equation for the axis ratios of the ellipsoid (*Holsapple,* 2010, equation (45)), which can be numerically integrated. A typical result is presented in Fig. 5, which plots the axis ratios along level sets of solutions to the differential equations.

For an object starting in the upper right corner of this figure, which represents a slightly oblate initial shape, the body will flatten, becoming more oblate. It can ideally approach a very flat shape with thickness only a fraction of its diameter before then deforming to a prolate shape. For a body initially at a shape near the center of this plot, it will become more prolate, eventually approaching a very long shape, with a/c of 5.1 or more. As it deforms, although its angular momentum increases, in most cases its spin decreases because its moment of inertia increases. The implication of this is important for

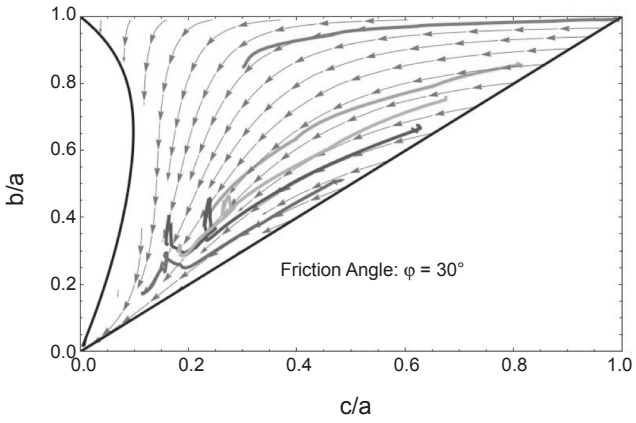

Fig. 5. Figure showing the deformation path of the semi-major axis ratios of an ellipsoid as its angular momentum is increased. An object with the angle of friction of 30° can be at its limit spin at any point along one of the curves in this figure. If the angular momentum is slowly increased, e.g., by YORP, the object deforms and traces a path in the direction indicated along the curves shown. The overlain lines show results of numerical simulations using a SSDEM model. From *Sánchez and Scheeres* (2012). These curves terminate when the body fissions, which is not modeled in the analytical theory.

interpreting the spin limit in Fig. 3. It predicts that bodies that lie at the minimum spin period line may not necessarily be at the limit of their angular momentum, but may be starting to go through a deformation that may actually decrease their spin rate as their angular momentum increases.

These deformational dynamics have also been seen in numerical simulations. *Walsh et al.* (2008) analyzed the effect of spinup on initially spheroidal rubble piles modeled with an HSDEM code. They found that as spin increased, components of the body would migrate to the equator, both causing a bulge to form and leading to loss of components into orbit about the body. These studies indicated a link between the expected shape deformation from YORP spinup and with these bodies being linked to binary formation. *Sánchez and Scheeres* (2012) also analyzed such spinup deformations using an SSDEM code. Their numerically computed deformations are plotted in Fig. 5 and are seen to closely follow the analytical curves derived by *Holsapple* (2010). However, we note that these simulations are only started in ellipsoidal shapes and are not constrained to be ellipsoidal (unlike the Holsapple computations). Thus as the angular momentum becomes large enough, the collections of grains are seen to undergo deformation beyond the classical ellipsoid shape. This is seen as the sequence of ideal ellipsoid deformations end once they become unstable and sensitive to collapse, which occurs at extreme elongations. The manner in which such systems fail range from surface shedding to fission, and is largely driven by the morphology of the mass distribution. Specifically, in the *Sánchez and Scheeres* (2012) simulations, initially ellipsoidal bodies are found to separate due to fission while initially spherical bodies are seen to shed material from their surface. Another possible outcome of deformation is a change in the body's YORP coefficient, which can cause a body's spin evolution to change sign, as initially noted in *Scheeres et al.* (2007) and recently studied in detail in *Statler* (2009) and *Cotto-Figueroa et al.* (2015).

Strongly oblate shapes have been found in several asteroids, some of which are fast rotating, such as (66391) 1999 KW_4, (341843) 2008 EV_5, (367943) Duende (formerly 2012 DA_{14}), (101955) Bennu (formerly 1999 RQ_{36}), (65803) Didymos, (2867) Šteins, and others. The equators of these objects generally protrude outside the equivalent oblate ellipsoidal shape, and therefore loose particles at their equator can spin off (*Scheeres,* 2015). Such shed particles are found to eventually escape (*Jacobson and Scheeres,* 2011a), although if sufficient numbers are shed in a short period, they may also form into a secondary (*Walsh et al.,* 2008, 2012). Analytical studies of such spunup shapes have been published by *Harris et al.* (2009), *Minton* (2008), and most recently *Scheeres* (2015). These studies seek to tie surface deformation to the overall shape of the body, with a particular focus on the oblate, fast-spinning shapes that have been associated with primaries of binary asteroids.

4.4. Evidence for Fission

One predicted outcome for rapidly spinning bodies is that they can undergo a shape bifurcation and separation into multiple components. This outcome is to be compared to the loss of material directly from the surface — a distinction that has been studied to some extent in *Walsh et al.* (2008), *Hirabayashi and Scheeres* (2014), and *Hirabayashi* (2014). Analytical methods applied to simplified studies have been able to model such fission mechanics. In *Scheeres* (2009a) it was shown that the first components to fission in a non-uniform body will be those whose mass centers are the furthest from each other. For simple models of ellipsoids resting on each other, this corresponds to the distinct bodies fissioning first. Under this assumption, it is possible to show that the dynamical evolution of a fissioned body can be directly related to the relative mass fraction between the components (*Scheeres,* 2007, 2009b). Specifically, if the mass ratio between the bodies is less than ~0.2, the resulting system has positive total energy and can escape [albeit not immediately (*Jacobson and Scheeres,* 2011a)], while for mass ratios larger than this the bodies are gravitationally bound and cannot escape without exogenous forcing.

This theory was specifically supported with the observations from *Pravec et al.* (2010) on asteroid pairs, which are asteroids that have had an extremely close passage to each other at an extremely slow speed (<1 m s^{-1}) at some point in the past (*Vokrouhlický and Nesvorný,* 2008). In the Pravec survey the relative sizes of asteroid pairs were determined and the spin period of the primary measured (see Fig. 6). This survey showed the predicted relation between mass ratio and formation of asteroid pairs, as there is a cut-off in asteroid pairs for mass ratios larger than ~0.2. As a secondary confirmation, the analysis also showed that the spin rates of

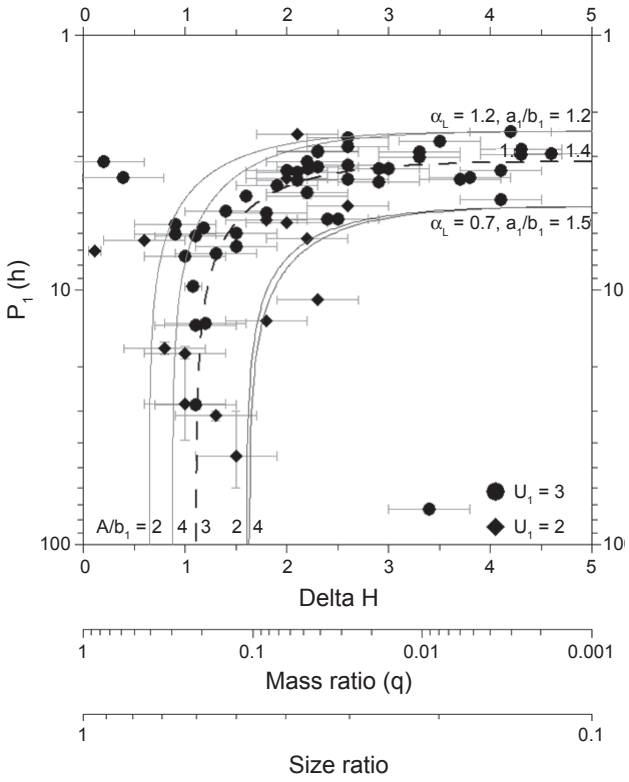

Fig. 6. Asteroid pairs showing the mass ratio and spin period of the primary with data through September 2014 (*Pravec,* 2014). There are a few significant outliers that do not fit with the theory, although the majority of added pairs is consistent with the initial interpretation in *Pravec et al*. (2010), where the parameters and detailed models used are described.

primaries decrease as the mass ratio limit is approached, which is the predicted mechanism for ejection, where energy for escape is taken from the spin rate of the primary. Additional observations of asteroid pairs have largely been consistent, although there are a few bodies that do not follow this rule and thus may be asteroid pairs formed by another mechanism (cf. *Vokrouhlický and Nesvorný,* 2008). There have also been spectroscopic studies of these asteroid pairs by *Polishook et al.* (2014), which have also been interpreted to support the fission hypothesis. This is significant as it has direct bearing on the manner in which rubble-pile bodies fail, even though there is not much detail. The implications of such fissioning have been investigated in *Jacobson and Scheeres* (2011a), which is described more fully in the chapter by Walsh and Jacobson in this volume.

4.5. Spin Limits for Cohesive Objects

Since *Asteroids III,* a significant number of small asteroids spinning above the limits derived for a cohesionless rubble pile have been discovered. Those objects, whose existence was predicted in *Harris* (1996), must have sufficient internal strength to withstand their internal tensile stresses. The question these bodies raise is what physics provide the source of that strength, what magnitude of strength is needed, and whether these can still be thought of as rubble-pile bodies.

That question was first addressed in *Holsapple* (2007), where the rubble-pile analysis outlined above was expanded to include strength models with cohesive strength, and it was found that the limit spins could be substantially faster if the internal material was capable of withstanding some level of tensile stress. However, that is true only for smaller asteroids, as can be seen in Fig. 3, as all the strength-limit curves fall back to the nominal spin limit for increasing size (which is the reason why the gravity spin limit does not necessarily imply cohesionless rubble piles). Holsapple derived specific limit curves for two strength cases. First, for a constant strength it is found that the maximum spin rate decreases linearly as the asteroid diameter increases, as noted in *Harris* (1996). Second, it was assumed that the strength of meter- to kilometer-sized objects will decrease with increasing size, to the –1/2 power, and in this way accounting for increasing planes of weakness in a larger body. Then the limits of spin vs. size decrease with the power of –5/4. The resulting curve is the upper, bounding curve plotted in Fig. 3. This curve furnishes an upper bound to all the present data and is for a material that has a tensile strength of only 100 kPa in a 10-cm specimen, and then decreasing as $1\sqrt{r}$ with size r. That value is more than an order of magnitude less than measured for typical meteorites (see section 2). Therefore, whether these data are really constrained by a strength limit or not remains an open question, as the limit may only indicate a lack of mechanism to further increase spin rates. A related question is also whether this represents the strength of individual components.

Sánchez and Scheeres (2014) have investigated the question of what minimum level of strength could exist between rubble-pile components. It is an important distinction that they are not considering the strength of all components, but are probing for the presence of possible cohesive strength between rubble-pile components. Their theory notes that van der Waals attractions between the finest material present in the rubble pile (in sufficient quantities to form an underlying matrix of material) should hold larger components in place, in the same way that cement holds rocks within a matrix. Using data from the Apollo lunar experiments and samples, and information on size distributions inferred from observations and samples from Itokawa, they predict the possible strength of this regolith to be on the order of 100 Pa, with their preferred value stated as 25 Pa (it should be noted that this value depends on an assumed density, angle of friction, and other shape parameters). This model probes the lower end of the strength envelope to determine whether there is any evidence for such cohesive strength in rubble-pile asteroids.

Sánchez and Scheeres (2014) point to a few aspects of the asteroid size, spin, and morphology database represented in Fig. 3, in addition to some specific asteroids, as evidence for their theory. First they note that cohesive strength between rubble-pile components greater than ~100 Pa should

lead to a more filled-in population below the strength line in the intermediate size range of 0.1–1 km. However, only when total effective strength (which is actually a function of density and shape assumptions as well) falls below the 100-Pa limit is the visual gap less significant. Another prediction from this theory is that binaries should not form when less than a certain size, as the spin rate required for fission to overcome cohesion would cause the resulting fragments to separate at speeds in excess of their mutual gravitational escape speed. They use this to explain the sharp drop-off in binaries below a few hundred meters, which has been shown to be statistically significant (see the chapter by Margot et al. in this volume). Finally, the presence of small and rapidly spinning tumbling asteroids at the strength limit is also consistent with the failure of rubble-pile asteroids with cohesion, as such a failure will generally induce tumbling in the separated bodies, which will also immediately escape from each other (*Scheeres et al.,* 2010). There are also a few specific bodies that provide additional support for this weak level of strength being present in a rubble-pile body. These are P/2013 R3, (29075) 1950 DA, and 2008 TC_3, which are discussed in the final section.

Before continuing it is important to note that the apparent gap between strengths greater than 100 Pa and the observed bodies in the 0.1–1-km range has been challenged by a number of observations that show the existence of objects that fill in the region beneath the upper bound. These are noted in *Holsapple* (2007) and reported in *Masiero et al.* (2009), *Chang et al.* (2014), and *Urakawa et al.* (2014). These observations have not been deemed sufficiently reliable in the lightcurve database (*Warner et al.,* 2009) to include in the confirmed cases. It is important that these objects be viewed in future apparitions to confirm them. Confirmation of these bodies' size and spin rates would have a significant impact on our understanding of the possible strength of asteroids.

5. PROBING ASTEROID INTERIORS

Although the previous models and interpretations take the interior properties of asteroids into account, they do not directly sense or constrain the interior properties or geophysics. This is because they still rely on external measures of the asteroid stability state, such as its shape, size, and spin. This section discusses approaches that are currently being developed to probe the interior properties of an asteroid, taking advantage of fundamental geophysical properties and observable effects. There are three main recent advances in this area, the first of which is the classical interpretation of surface geological structures to make inferences on the interior of an asteroid. Second is the analysis of the interior seismic properties of rubble-pile bodies. Third is the analysis of tidal dissipation effects within small rubble-pile bodies. A fourth advance that can be mentioned in passing is the use of radar to probe the interior of a rubble-pile body. However, there have not been definitive analyses of this approach for asteroidal bodies, although such analyses will be performed for the first time at a comet by the Rosetta spacecraft.

5.1. Geological Interpretation

The classical approach to interpreting the interior structure of an asteroid was pioneered at the asteroid (433) Eros, although it has also been applied to interpret the interior of Phobos (see the chapter by Marchi et al. in this volume). The underlying theory is outlined in *Prockter et al.* (2002) and interprets surface features as expressions of subsurface strength. The key focus was on the lineaments and global structures such as Rahe Dorsum on Eros. *Buczkowski et al.* (2008) studied the lineaments across Eros to determine whether there was clear evidence for internal strength or structures. While certain correlations seem to exist, along with evidence for some subsurface structure, it is also difficult to independently confirm what these structures may be, whether they arise from the mechanical properties of the regolith itself, or how they could be uniquely estimated (*Robinson et al.,* 2002). The approach has also had limited use at (25143) Itokawa, where there are no specific global geographic features that could be used to make interior interpretations other than the component shapes themselves. On the other hand, such an approach can be very valuable at a larger body such as (4) Vesta, which has many global features that could be used as constraints on the interior of the body (reviewed in the chapter by Russell et al. in this volume).

5.2. Seismic Effects

The importance of seismic effects was underlined by the Near Earth Asteroid Rendezvous (NEAR) observations of Eros. While craters were present on that body, they became more sparse at smaller sizes, with the surface dominated by a thick layer of regolith (*Chapman et al.,* 2002). This was explained using a statistical and global analysis of crater erasure due to seismic shaking as a result of impacts on Eros (*Richardson et al.,* 2004). In a subsequent analysis, *Thomas and Robinson* (2005) were able to positively correlate the erasure of small craters with a single large impact, thus linking the transmission of seismic energy from an impact to the surface motion of regolith and not due to regolith created in the impact itself. The chapter by Marchi et al. in this volume reviews this material in more detail.

Motivated by, and contemporaneous with, this physical correlation there were many different studies of the effects of impacts on the redistribution of regolith. These include the use of particle hydrodynamic codes for simulating impacts (*Nolan et al.,* 2001), coupled models of seismic transmission and granular motion (*Richardson et al.,* 2004; *Richardson and Bowling,* 2014), and the application of Earth geophysical models of seismic-energy transmission to rubble-pile bodies (*Martin et al.,* 2008; *Blitz,* 2009).

A culmination of these analyses is the realization that the mechanical properties of a rubble-pile body can be linked with the observed crater distributions and levels of erasure. *Asphaug* (2008) proposes a methodology to directly estimate the attenuation of seismic energy within a rubble pile using the observed largest crater on that body. This basic idea has

also migrated beyond the use of naturally occurring impacts to include the application of controlled and induced cratering blasts or impacts on the surface of a rubble-pile asteroid. By controlling the energy and deposition of the blast, it is possible to infer the seismic transmission of energy at distal points of a rubble-pile body by comparing before and after images of the surface. This can be enhanced by the deployment of instrumented devices across the surface, where they can record the sensed seismic energy or, in the extreme case if they are lofted from the surface, determine the strength of the seismic wave by tracking the length of their ballistic phase. Such ideas were proposed in *Scheeres et al.* (2003) and have subsequently appeared as a concept in a number of space science missions, with the combination of calibrated blasts and sensing measuring devices proposed in the Discovery mission Binary Asteroid In-Situ Explorer (BASiX) (*Robert et al.,* 2010). Similar concepts have also been subsequently proposed in the mission concepts of MarcoPolo-R (*Michel et al.,* 2014) and Asteroid Impact and Deflection Assessment (AIDA) (*Galvez et al.,* 2013). This approach to seismic inference will be realized with the currently planned Hayabusa-2 mission to primitive asteroid 1999 JU_3. This mission concept calls for using an explosive device to accelerate an impactor into the surface of the body, creating a crater and seismic energy source that can then be tracked by observing modifications of the surface (*Tsuda et al.,* 2013).

5.3. Tidal Dissipation

Another measure that can used to peer into the interior of a rubble-pile body is related to energy dissipation due to tidal deformations. There are two main ways in which rubble-pile bodies can dissipate excess kinetic energy via this method. One occurs if the body is in a non-uniform rotation state, as this induces traveling waves of alternating accelerations, which can cause stress and strains that dissipate energy. This effect has been linked to the fact that the vast majority of asteroids are in or near a rotation state about their maximum moment of inertia (*Burns and Safronov,* 1973). *Harris* (1994) showed that the vast majority of known tumbling asteroids had an overall slow rotation rate, meaning that the time for them to relax to uniform rotation could be long, although these estimates depend on assuming that the geophysical properties of larger planetary bodies and satellites are similar to rubble-pile bodies.

To better constrain and understand how the observed tumblers should be interpreted in terms of their internal geophysics of tidal dissipation, there have been several analytical and numerical studies of how asteroids could enter complex rotation states and what the frequency of them entering such states should be. This would allow for the comparison of the population with different dissipation rates. The trend of tumbling with greater spin period implicitly indicates that asteroids are dissipative bodies. The degree of dissipation is not fully understood, and depends on the assumed parameters of rigidity, μ, which measures the stiffness of the body; the quality factor, Q, which is inversely proportional to the rate of energy dissipation due to non-uniform deformations; and the rate at which tumblers are created. We note that tumblers can be created in several ways: catastrophic disruptions (*Asphaug and Scheeres,* 1999; *Scheeres et al.,* 2000b), planetary flybys (*Scheeres et al.,* 2000b, 2005; *Pravec et al.,* 2014), YORP-induced fission (*Sánchez and Scheeres,* 2014), and, potentially, YORP spindown effects either in isolation (*Vokrouhlickỳ et al.,* 2007) or in combination with impacts (*Marzari et al.,* 2011; *Henych and Pravec,* 2013).

On the other hand, the application of standard planetary theory geophysics to rubble-pile asteroids made in earlier studies may not be appropriate. This has motivated researchers to develop improved mathematical models and to carry out geophysical analyses that are relevant for this environment. *Efroimsky and Williams* (2009) considered the effect of frequency dependent terms in tidal dissipation, while *Sharma et al.* (2005) and *Breiter et al.* (2009) have developed novel mathematical expressions for tidal dissipation. Perhaps most fundamental, however, is the study by *Goldreich and Sari* (2009), which shows that rubble-pile bodies are expected to behave distinctively relative to the classical planetary satellite theory. In their analysis they show that the functional relationship between the quality factor, Q, and the Love number of an object, k (related to the rigidity of the body and how the shape responds to tidal stress), should follow a variation where $Q/k \propto r$, the radius of the body, which is distinctly different than the classical relationship. Specifically, they show that the effective dimensionless rigidity of a rubble pile is smaller than that of a monolithic body of the same size, with the reduction arising from the concentration of stresses due to the presence of voids. Using this result they show that it is likely that a rubble-pile secondary in a binary asteroid system should circularize, which cannot be necessarily concluded if the secondary is monolithic and follows the classical planetary relation. The implications of their analysis for the relaxation time for tumbling asteroids has not been made as of yet.

The Goldreich and Sari analysis has been applied to develop a more detailed model for the expected evolution of binary asteroid systems. In *Jacobson and Scheeres* (2011b) they analyze the joint evolutionary dynamics of tidal dissipation and the binary YORP (BYORP) effect (see the chapter by Vokrouhlický et al. in this volume) in light of the Goldreich and Sari theory for tidal dissipation. They find that there should exist a so-called BYORP and tide equilibrium where a contractive BYORP effect acting on the synchronous secondary is balanced by an expansive tidal effect due to dissipation in the rapidly rotating primary. The existence of this equilibrium is significant for a number of reasons, described elsewhere in this volume in the chapters by Walsh and Jacobson and Vokrouhlický et al. In the context of this chapter the significance is that this provides a direct way in which to constrain and indirectly measure the rigidity of the primary in a rubble-pile binary asteroid. Once a binary asteroid is known or suspected to lie in such an equilibrium, it also provides a way to evaluate the functional relationship between a body's size and its quality factor and tidal

Love number. The existence of this equilibrium has been recently validated for binary asteroid 1996 FG_3 (*Scheirich et al.,* 2015). From that study there is an inferred value of rigidity times quality factor of $\mu Q \sim 2.7 \times 10^9$ Pa, which is orders of magnitude less than that expected for a monolithic body and for what has been bounded in the past for binary asteroids (*Margot et al.,* 2002). This result is significant, as it is the first "measured" value of this parameter for a rubble-pile body, albeit there are a number of significant sources of uncertainty that are discussed in that paper.

A significant next step in analysis will be to start to blend these results to better understand the dissipation rate within rubble-pile bodies. This will require additional theoretical, observational, and ultimately numerical computations to fully understand. It also provides motivation for a space science mission to a binary asteroid in a BYORP-tide equilibrium, since obtaining a precise estimate of the rigidity requires that the secondary body be fully mapped.

6. SPECIFIC ASTEROID OBSERVATIONS

In addition to the insights obtained by analyzing the asteroid population database, there have been significant insights from analyzing specific asteroids. There have been a number of dramatic and unprecedented observations of single bodies that provide deep insight into the morphology and, in some cases, the mechanical properties of these asteroids. In the following we discuss some of the more significant of these bodies. As some of these bodies are discussed in more detail elsewhere, in some cases we only draw on a few aspects of the analysis and indicate the appropriate chapter for more details. Instead of grouping these bodies by how they were observed, which could be done, we just list them in order of their alphabetical names and designations.

6.1. (433) Eros

At the time the *Asteroids III* book was being completed, significant, but incomplete, data on asteroid (433) Eros taken by the NEAR-Shoemaker spacecraft was already included. The definitive analysis of the gravity field of this asteroid had not been published, however, and is what we focus on here. Initial data indicated that the asteroid's gravity field was homogeneous at the few-kilometers scale (*Asphaug et al.,* 2002). Subsequent analysis of the gravity field was made and reported in two papers (*Miller et al.,* 2002; *Konopliv et al.,* 2002). Both papers included a comparison between the measured gravity field and a homogenous gravity field computed from the shape with a constant density assumption. Density variations can be detected through the comparisons of measured and computed gravity field coefficients (cf. *Scheeres et al.,* 2000a; *Takahashi and Scheeres,* 2014). Gravity field comparisons in both papers showed differences at the relative level of less than 10^{-3} through the 6th degree-and-order gravity terms. At higher degree and order the uncertainty in the gravity-field coefficients was greater than this relative level, meaning that at these higher levels the differences were indistinguishable from noise. This provides a strong constraint on the density homogeneity within this asteroid. We also note that the bulk density of this body was determined to be 2.67 ± 0.03 g cm^{-3} (*Miller et al.,* 2002), indicating a relatively low level of macroporosity of approximately 20% assuming the S-type asteroid had a grain density of ordinary chondrites (*Yeomans et al.,* 2000). The *Miller et al.* (2002) paper also made an accurate rotation-state estimate for the body, and was unable to observe any complex rotation except that driven by solar torques. This indicates that the body had fully relaxed to principle-axis rotation.

6.2. (25143) Itokawa

The asteroid (25143) Itokawa was visited by the Hayabusa spacecraft in 2005 (see the chapter by Yoshikawa et al. in this volume). The greatest achievement of that mission was the collection of a small but valuable sample of regolith from the surface. However, several important observations and measurements of the asteroid were also taken during the few months that the spacecraft was in close proximity to that body. There were several important determinations with regard to the geophysics of this asteroid. These include the total bulk density of the body, measured to be 1.9 ± 0.13 g cm^{-3}, corresponding to a macroporosity of 41% for this S-type asteroid (*Fujiwara et al.,* 2006). As the spacecraft never spent significant time in ballistic motion close to the asteroid, the gravity field determination was not able to progress beyond the total mass. Subsequent to the mission it has been speculated that the density distribution within the body is heterogeneous. This idea was first proposed in *Scheeres and Gaskell* (2008) to explain the apparent disconnect between the predicted YORP torque (which was computed to be negative based on several different computations) and the lack of a detected change in its spin. This theory predicted that either the head or neck region of the body should have a greater density. *Lowry et al.* (2014) were able to detect a measurable acceleration in the spin rate of Itokawa. Based on the theory outlined in *Scheeres and Gaskell* (2008) and *Breiter et al.* (2009) it was determined that the density disparity between the head and body would need to be 2.85 and 1.75 g cm^{-3}, respectively, for this effect alone to account for the disparity. Such a drastic disparity between densities, 62%, is not out of the question given that the secondary and primary of (66391) 1999 KW_4 have a large density disparity, although for that body it is only 42% for the nominal values (see below). However, as discussed in the chapter by Vokrouhlický et al. in this volume, there are other effects besides a density disparity that could have caused the acceleration of Itokawa, making the result somewhat uncertain.

Beyond the mass, bulk density, macroporosity, and possible density heterogeneity, important information was obtained regarding the size distribution of rocks, boulders, and grains on Itokawa. Based on images taken while in close proximity to the body, the size distribution of boulders and rocks across its surface was measured and found to follow a size distribution with an exponent of -3.1 ± 0.1 down to

5 m (*Michikami et al.,* 2008). A more recent paper revisits the Itokawa data and focuses on the difference between the head and body of this asteroid, as well as discussing several possible hypotheses for its formation (*Mazrouei et al.,* 2013). They find a somewhat steeper size distribution down to 6 m, albeit changing depending on where on the body one looks. Ultimately their general conclusions on the distribution of larger blocks are consistent with *Michikami et al.* (2008). Using the returned samples, a size-distribution analysis was also made by *Tsuchiyama et al.* (2011). Across the grain sizes ranging from 0.5 to 100 μm they found a size distribution with an exponent between –2.8 and –2 (steeper at the smaller sizes). While these two size distributions (from the observations and the samples) cannot be easily combined, they do present some insight into the size distribution of grains and boulders within a rubble-pile asteroid. Tscuchiyama et al. present the hypothesis that the size distribution may break to a shallower level at millimeter- to centimeter-sized grains, which may explain why they were viewed as the dominant grain size on the body [at least in the Muses-Sea region (*Yano et al.,* 2006)]. These measurements of size distribution are important as they speak directly to the presumed size distributions that all rubble-pile bodies may have. Also, the recent theory on cohesive strength in rubble piles (*Sánchez and Scheeres,* 2014) depends explicitly on the presence of fine regolith grains for its physical realization.

6.3. (216) Kleopatra

The asteroid (216) Kleopatra is a strangely shaped main-belt asteroid with a total length on the order of 250 km and with a very narrow "neck" (*Ostro et al.,* 2000). This asteroid has already been distinguished by its rapid rotation and odd shape. *Descamps et al.* (2011) reported the discovery of two satellites about this asteroid, enabling a precise mass of the asteroid to be determined. However, while their observations were also consistent with the *Ostro et al.* (2000) radar-based shape, they reported finding a significantly larger size for this body, approximately 25% larger in mean diameter than the Ostro et al. radar shape. A different set of observations by *Marchis et al.* (2012) reported an even larger size, raising the interesting situation of knowing the mass and shape of the body but not its size and hence density. The rapid rotation of this object and its shape mean that the stability of this body is highly sensitive to its bulk density and size. *Hirabayashi and Scheeres* (2014) took advantage of this size ambiguity to probe the stability of this body across a range of sizes, from the *Ostro et al.* (2000) size to the *Marchis et al.* (2012) size. Based on an averaged stress analysis, essentially applying the averaging method of Holsapple to a non-ideal shape, they were able to determine that the *Descamps et al.* (2011) size requires the lowest angle of friction to keep the body stable. This analysis has also been confirmed using a finite-element plastic-deformation analysis that shows that the smaller *Ostro et al.* (2000) size will tend to collapse, the larger *Marchis et al.* (2012) size will tend to separate, and the *Descamps et al.* (2011) size seems to be the most stable again, and is only susceptible to surface failures that could be related to inaccuracies in the detailed shape of the body (*Hirabayashi,* 2014). This analysis is listed here as it represents a unique use of continuum and failure theory to help resolve an inconsistency in measurements.

6.4. (29075) 1950 DA

The asteroid (29075) 1950 DA is well known as one of the most hazardous bodies for Earth in the solar system, due to its relatively high impact probability of 1 in 4000 (albeit in the year 2880) and its relatively large size, on the order of 1 km (see the chapter by Harris et al. in this volume). In *Rozitis et al.* (2014) the body's density is determined by using the measured Yarkovsky acceleration of the body and analyzing the thermal inertia. This allowed them to infer that the body was a rubble pile, that the rotation of the body was retrograde, and that the corresponding shape model for this rotation pole could be used (*Busch et al.,* 2007). Based on these measurements, *Rozitis et al.* (2014) determined that the body was spinning beyond the failure limit at which both loose material would be shed from its surface and it would undergo global deformation. Due to this they concluded that the body required cohesion to stay intact, and applied basic techniques (*Holsapple,* 2001) to determine the level of cohesive strength needed. Based on a Drucker-Prager failure model they were able to identify a minimum necessary strength of approximately 65 Pa for the body to hold together, which they note is comparable to the level of strength for rubble-pile bodies hypothesized in *Sánchez and Scheeres* (2014). A detailed finite-element analysis was performed by *Hirabayashi and Scheeres* (2015) that confirmed this strength as a lower bound and found that for uniform strength, the center of the body should fail prior to the surface. They note that should this occur, it could result in a less-dense core, which could be detected with an orbiting spacecraft.

6.5. (66391) 1999 KW_4

The binary asteroid (66391) 1999 KW_4 was observed with range-Doppler radar at a number of epochs, enabling a detailed model of the shapes of each of its components and their relative orbital and rotational dynamics *(Ostro et al.,* 2006; *Scheeres et al.,* 2006). These papers provided the first, and to date most accurate, insight into the morphology of a binary asteroid system, and it is of interest to briefly review the results here. First, it is important to note that in the nominal model the primary rotates just shy of where loose material should be shed from its surface, implying that its interior may also be close to a failure limit. At the lower end of density for the primary the surface may require cohesive strength to stay together. Thus this body exhibits and showcases the traits of the rapidly rotating oblate bodies discussed earlier in this chapter and has been used as the motivating example of this class of body (*Harris et al.,* 2009; *Scheeres,* 2015).

The primary has an obliquity of about 3° with respect to the orbit plane of the binary and the secondary has relative

librations of several degrees. Thus the system is not in a fully relaxed state. Based on the shape of the secondary we note that the predicted BYORP coefficient is positive, meaning that this system could be undergoing expansion (the system is currently being monitored for BYORP expansion, as described in the chapter by Vokrouhlický et al. in this volume). As this system has not settled into a fully relaxed state it introduces the interesting possibility that it could be tracked over longer time periods to possibly determine or detect effects associated with either tidal relaxation or with BYORP expansion.

There is a large density disparity between the primary and secondary body. The primary density is determined to be 1.97 ± 0.24 g cm^{-3} and the secondary to be $2.81^{+0.82}_{-0.63}$ g cm^{-3}, a relative factor of 42%. Possible reasons for such a disparity are discussed in *Scheeres et al.* (2006), and involve the compaction of the secondary by continuous shaking and the expansion of the primary due to the extremely rapid rotation rate.

6.6. 2008 TC_3

Now we consider asteroid 2008 TC_3, which became the Almahata Sitta meteorite (*Jenniskens et al.,* 2009). This asteroid was observed prior to entering Earth's atmosphere during the brief period after its discovery. Lightcurve observations of this body showed that it was spinning with a period of 100 s and also was in a tumbling rotation state (*Scheirich et al.,* 2010). It can be found on Fig. 3, where it is the smallest known tumbler and only requires approximately 100 Pa of cohesive strength to withstand disruption. Based on analysis of the meteorite fall, this body consisted of several different mineralogical types that constituted separate components in the parent asteroid (see the chapter by Jenniskens in this volume), with one possible interpretation being that it could be described as a rubble pile (*Jenniskens et al.,* 2009). Analysis of the preentry observations and the meteorite falls also indicate that the body had significant macroporosity (*Kohout et al.,* 2011). The meteor was observed to break up high in the atmosphere, indicating a weak body (*Borovička and Charvat,* 2009; *Popova et al.,* 2011). Furthermore, *Borovička and Charvat* (2009) note the presence of an abundance of micrometer- and larger-sized dust associated with the meteor, consistent with this dust composing a "substantial part" of the total mass of the object. These disparate observations related to this asteroid were linked together in the recent theory proposed in *Sánchez and Scheeres* (2014), and described earlier in section 4.5, although there remain questions about that interpretation (see discussion in the chapter by Borovička et al. in this volume).

6.7. P/2013 P5

Body P/2013 P_5 was initially catalogued as a comet, yet now seems to more properly identified as an asteroid (see the chapter by Jewitt et al. in this volume; *Jewitt et al.,* 2013; *Hainaut et al.,* 2014). This body has exhibited periodic shedding over a number of different observational epochs. Material shed from its surface has been seen to consist of fine grains down to 10 μm in size at least. A clear explanation for its periodic shedding has not been found, although some initial analysis of this phenomenon has occurred (*Scheeres,* 2015).

6.8. P/2013 R3

Finally, we mention another active asteroid, P/2013 R_3 (*Jewitt et al.,* 2014). This body was seen to fail in an entirely different morphological fashion, splitting repeatedly into smaller components that escaped from each other. *Hirabayashi et al.* (2014) analyzed the main components of this body and estimated the initial spin rate of the protobody by mapping estimates of size and speed backward to the inferred epoch of disruption. Based on this analysis they predicted a range of possible strengths for the progenitor rubble-pile body prior to breakup, from 40 to 200 Pa, with the range of values accounting for uncertainties in size, density, and relative speed.

7. CONCLUSIONS

In this chapter we bring together disparate material on the strength, mechanics, and morphology of asteroids based on meteors and meteorites, groundbased observations, spacebased observations, analysis, and numerical simulation. While there has been significant progress on all fronts since *Asteroids III*, many new issues and questions have been exposed as well. A main issue that arises is the wide variation in strength determinations of asteroids and their constituents. While direct comparisons of meteor strengths as parameterized by dynamic pressure and strength parameterized by spin rate cannot be naively made, there must be some underlying connection between these. Elucidation of this should be a priority, as it would enable a clear application of meteor data to the interpretation of strength of rubble-pile bodies. Another area that is ripe for progress is an improved theory of tidal dissipation within rubble-pile bodies, coupled with new ways in which the fundamental parameters of rubble piles can be estimated. This involves a better understanding of how asteroids are made to tumble, modified theories for tidal dissipation of rubble-pile bodies, and estimation of improved values for rigidity, tidal Love number, and quality factors of rubble piles. Finally, the continued advancement in analytical and numerical simulation tools will be essential for continued progress in this difficult and fundamental issue of asteroid mechanics.

Acknowledgments. D.J.S. acknowledges support from the NASA Near Earth Object Observations Program through grant NNX14AL16G. The authors appreciate the thorough reviews from two expert referees.

REFERENCES

Abe S., Mukai T., Hirata N., et al. (2006) Mass and local topography measurements of Itokawa by Hayabusa. *Science, 312,* 1344–1347.

Asphaug E. (2008) Critical crater diameter and asteroid impact seismology. *Meteoritics & Planet. Sci., 43,* 1075–1084.

Asphaug E. and Scheeres D. J. (1999) Deconstructing Castalia: Evaluating a postimpact state. *Icarus, 139(2),* 383–386.
Asphaug E., Ryan E. V., and Zuber M. T. (2002) Asteroid interiors. In *Asteroids III* (W. F. Bottke Jr. et al., eds.), pp. 463–484. Univ. of Arizona, Tucson.
Bendjoya P. and Zappalà V. (2002) Asteroid family identification. In *Asteroids III* (W. F. Bottke Jr. et al., eds.), pp. 613–618. Univ. of Arizona, Tucson.
Blitz C. (2009) Modélisation de la propagation des ondes sismiques et des ejecta dans les astéroides : Application à lérosion des cratères de lastéroide (433) Eros. Ph.D. thesis, Institut de Physique du Globe de Paris, Paris.
Borovicka J. and Charvat Z. (2009) Meteosat observation of the atmospheric entry of 2008 TC3 over Sudan and the associated dust cloud. *Astron. Astrophys., 507(2),* 1015.
Borovička J. and Spurnỳ P. (2008) The Carancas meteorite impact — Encounter with a monolithic meteoroid. *Astron. Astrophys., 485(2),* L1–L4.
Borovička J., Spurnỳ P., Brown P., et al. (2013) The trajectory, structure and origin of the Chelyabinsk asteroidal impactor. *Nature, 503,* 235–237.
Brearley A. J. and Jones R. H. (1998) Chondritic meteorites. *Rev. Mineral. Geochem., 36(1),* 3–1.
Breiter S., Bartczak P., Czekaj M., et al. (2009) The YORP effect on 25143 Itokawa. *Astron. Astrophys., 507(2),* 1073.
Britt D. T., Yeomans D. K., Housen K. R., and Consolmagno G. J. (2002) Asteroid density, porosity, and structure. In *Asteroids III* (W. F. Bottke Jr. et al., eds.), pp. 485–500. Univ. of Arizona, Tucson.
Brown P. G., Revelle D. O., Tagliaferri E., and Hildebrand A. R. (2002) An entry model for the Tagish Lake fireball using seismic, satellite and infrasound records. *Meteoritics & Planet. Sci., 37(5),* 661–675.
Buczkowski D. L., Barnouin-Jha O. S., and Prockter L. M. (2008) 433 Eros lineaments: Global mapping and analysis. *Icarus, 193(1),* 39–52.
Burns J. A. and Safronov V. S. (1973) Asteroid nutation angles. *Mon. Not. R. Astron. Soc., 165,* 403.
Bus S. J. and Binzel R. P. (2002) Phase II of the Small Main-Belt Asteroid Spectroscopic Survey: A feature-based taxonomy. *Icarus, 158,* 146–177.
Busch M. W., Giorgini J. D., Ostro S. J., et al. (2007) Physical modeling of near-Earth asteroid (29075) 1950 DA. *Icarus, 190(2),* 608–621.
Carruba V., Domingos R. C., Nesvorný D., et al. (2013) A multidomain approach to asteroid families' identification. *Mon. Not. R. Astron. Soc., 433,* 2075–2096.
Carry B. (2012) Density of asteroids. *Planet. Space Sci., 73,* 98–118.
Chandrasekhar S. (1969) *Ellipsoidal Figures of Equilibrium.* Dover, New York.
Chang C.-K., Waszczak A., Lin H.-W., et al. (2014) A new large super-fast rotator: (335433) 2005 UW163. *Astrophys. J. Lett., 791(2),* L35.
Chapman C. R., Merline W. J., Thomas P. C., et al. (2002) Impact history of Eros: Craters and boulders. *Icarus, 155(1),* 104–118.
Chree C. (1895) The equilibrium of an isotropic elastic solid ellipsoid under the action of normal surface forces of the second degree, and bodily forces derived from a potential of the second degree. *Q. J. Pure Appl. Math., 27,* 338–353.
Consolmagno G. J., Britt D. T., and Macke R. J. (2008) The significance of meteorite density and porosity. *Chem. Erde–Geochem., 68(1),* 1–29.
Cotto-Figueroa D., Statler T. S., Richardson D. C., and Tanga P. (2015) Coupled spin and shape evolution of small rubble-pile asteroids: Self-limitation of the YORP effect. *Astrophys. J., 803,* 25.
DeMeo F. E., Binzel R. P., Slivan S. M., and Bus S. J. (2009) An extension of the Bus asteroid taxonomy into the near-infrared. *Icarus, 202,* 160–180.
Descamps P., Marchis F., Berthier J., et al. (2011) Triplicity and physical characteristics of asteroid (216) Kleopatra. *Icarus, 211(2),* 1022–1033.
Dobrovolskis A. R. (1982) Internal stresses in Phobos and other triaxial bodies. *Icarus, 52(1),* 136–148.
Efroimsky M. and Williams J. G. (2009) Tidal torques: A critical review of some techniques. *Cel. Mech. Dyn. Astron., 104(3),* 257–289.
Fienga A., Manche H., Laskar J., and Gastineau M. (2008) INPOP06: A new numerical planetary ephemeris. *Astron. Astrophys., 477(1),* 315–327.
Fujiwara A., Kawaguchi J., Yeomans D. K., et al. (2006) The rubble-pile asteroid Itokawa as observed by Hayabusa. *Science, 312,* 1330–1334.
Galvez A., Carnelli I., Michel P., et al. (2013) AIDA: The asteroid impact and deflection assessment mission. In *European Planetary Science Congress, 8,* EPSC2013-1043. *Available online at http://meetings. copernicus. org/epsc2013*.
Grady M. M. (2000) *Catalogue of Meteorites, 5th edition.* Cambridge Univ., Cambridge.
Goffin E. (2014) Astrometric asteroid masses: A simultaneous determination. *Astron. Astrophys., 565,* A56.
Goldreich P. and Sari R. (2009) Tidal evolution of rubble piles. *Astrophys. J., 691,* 54–60.
Hainaut O. R., Boehnhardt H., Snodgrass C., et al. (2014) Continued activity in P/2013 P5 PanSTARRS. Unexpected comet, rotational break-up, or rubbing binary asteroid? *Astron. Astrophys., 563,* 75.
Harris A. W. (1994) Tumbling asteroids. *Icarus, 107(1),* 209–211.
Harris A. W. (1996) The rotation rates of very small asteroids: Evidence for 'rubble pile' structure. *Lunar Planet. Sci. XXVII,* p. 493. Lunar and Planetary Institute, Houston.
Harris A. W., Fahnestock E. G., and Pravec P. (2009) On the shapes and spins of rubble pile asteroids. *Icarus, 199(2),* 310–318.
Henych T. and Pravec P. (2013) Asteroid rotation excitation by sub-catastrophic impacts. *Mon. Not. R. Astron. Soc., 432(2),* 1623–1631.
Hilton J. M. (2002) Asteroid masses and densities. In *Asteroids III* (W. F. Bottke Jr. et al., eds.), pp. 103–112. Lunar and Planetary Institute, Houston.
Hirabayashi M. (2014) Structural stability of asteroids. Ph.D. thesis, University of Colorado, Boulder.
Hirabayashi M. and Scheeres D. J. (2014) Analysis of asteroid (216) Kleopatra using dynamical and structural constraints. *Astrophys. J., 780(2),* 160.
Hirabayashi M. and Scheeres D. J. (2015) Stress and failure analysis of rapidly rotating asteroid (29075) 1950 DA. *Astrophys. J. Lett., 798,* L8.
Hirabayashi M., Scheeres D. J., Sánchez D. P., and Gabriel T. (2014) Constraints on the physical properties of main belt Comet P/2013 R3 from its breakup event. *Astrophys. J. Lett., 789,* L12.
Holsapple K. A. (2001) Equilibrium configurations of solid cohesionless bodies. *Icarus, 154(2),* 432–448.
Holsapple K. A. (2004) Equilibrium figures of spinning bodies with self-gravity. *Icarus, 172(1),* 272–303.
Holsapple K. A. (2007) Spin limits of solar system bodies: From the small fast-rotators to 2003 EL61. *Icarus, 187,* 500–509.
Holsapple K. A. (2010) On YORP-induced spin deformations of asteroids. *Icarus, 205(2),* 430–442.
Housen K. R., Holsapple K. A., and Voss M. E. (1999) Compaction as the origin of the unusual craters on the asteroid Mathilde. *Nature, 402,* 155–157.
Hudson R. S., Ostro S. J., Jurgens R. F., et al. (2000) Radar observations and physical model of asteroid 6489 Golevka. *Icarus, 148(1),* 37–51.
Hudson R. S., Ostro S. J., and Scheeres D. J. (2003) High-resolution model of asteroid 4179 Toutatis. *Icarus, 161,* 346–355.
Jacobi C. G. J. (1834) Ueber die figur des gleichgewichts. *Ann. Phys., 109(8–16),* 229–233.
Jacobson S. A. and Scheeres D. J. (2011a) Dynamics of rotationally fissioned asteroids: Source of observed small asteroid systems. *Icarus, 214,* 161–178.
Jacobson S. A. and Scheeres D. J. (2011b) Long-term stable equilibria for synchronous binary asteroids. *Astrophys. J. Lett., 736(1),* L19.
Jenniskens P., Shaddad M. H., Numan D., et al. (2009) The impact and recovery of asteroid 2008 TC3. *Nature, 458(7237),* 485–488.
Jewitt D., Agarwal J., Weaver H., et al. (2013) The extraordinary multi-tailed main-belt comet P/2013 P5. *Astrophys. J. Lett., 778(1),* L21.
Jewitt D., Agarwal J., Li J., et al. (2014) Disintegrating asteroid P/2013 R3. *Astrophys. J. Lett., 784(1),* L8.
Kadish J., Barber J. R., and Washabaugh P. D. (2005) Stresses in rotating spheres grown by accretion. *Intl. J. Solids Structures, 42(20),* 5322–5334.
Kadish J., Barber J. R., Washabaugh P. D. and Scheeres D. J. (2008) Stresses in accreted planetary bodies. *Intl. J. Solids Structures, 45(2),* 540–550.
Kimberley J. and Ramesh K. T. (2011) The dynamic strength of an ordinary chondrite. *Meteoritics & Planet Sci., 46(11),* 1653–1669.
Kohout T., Kiuru R., Montonen M., et al. (2011) Internal structure and physical properties of the asteroid 2008 TC3 inferred from a study of the Almahata Sitta meteorites. *Icarus, 212(2),* 697–700.

Konopliv A. S., Miller J. K., Owen W. M., et al. (2002) A global solution for the gravity field, rotation, landmarks, and ephemeris of Eros. *Icarus, 160,* 289–299.
Kuchynka P. and FolknerW. M. (2013) A new approach to determining asteroid masses from planetary range measurements. *Icarus, 222,* 243–253.
Lowry S. C.,Weissman P. R., Duddy S. R., et al. (2014) The internal structure of asteroid (25143) Itokawa as revealed by detection of YORP spin-up. *Astron. Astrophys., 562,* 48.
Marchis F., Hestroffer D., Descamps P., et al. (2006) A low density of 0.8 g cm^{-3} for the Trojan binary asteroid 617 Patroclus. *Nature, 439,* 565–567.
Marchis F., Enriquez J. E., Emery J. P., et al. (2012) Multiple asteroid systems: Dimensions and thermal properties from Spitzer Space Telescope and ground-based observations. *Icarus, 221(2),* 1130–1161.
Margot J. L., Nolan M. C., Benner L. A. M., et al. (2002) Binary asteroids in the near-Earth object population. *Science, 296(5572),* 1445–1448.
Martin R., Komatitsch D., Blitz C., and Le Goff N. (2008) Simulation of seismic wave propagation in an asteroid based upon an unstructured mpi spectral-element method: Blocking and non-blocking communication strategies. In *High Performance Computing for Computational Science — VECPAR 2008* (J. M. Laginha et al., eds.), pp. 350–363. Springer-Verlag, Berlin.
Marzari F., Rossi A., and Scheeres D. J. (2011) Combined effect of YORP and collisions on the rotation rate of small main belt asteroids. *Icarus, 214(2),* 622–631.
Masiero J., Jedicke R., Ďurech J., et al. (2009) The thousand asteroid light curve survey. *Icarus, 204(1),* 145–171.
Masiero J. R., Mainzer A. K., Grav T., et al. (2011) Main belt asteroids with WISE/NEOWISE. I. Preliminary albedos and diameters. *Astrophys. J., 741,* 68.
Mazrouei S., Daly M. G., Barnouin O. S., et al. (2013) Block distributions on Itokawa. *Icarus, 229,* 181–189.
Michel P., Barucci M. A., Cheng A. F., et al. (2014) MarcoPolo-R: Near-Earth asteroid sample return mission selected for the assessment study phase of the ESA program cosmic vision. *Acta Astronaut., 93,* 530–538.
Michikami T., Nakamura A. M., Hirata N., et al. (2008) Size-frequency statistics of boulders on global surface of asteroid 25143 Itokawa. *Earth Planets Space, 60(1),* 13–20.
Miller J. K., Konopliv A. S., Antreasian P. G., et al. (2002) Determination of shape, gravity, and rotational state of asteroid 433 Eros. *Icarus, 155,* 3–17.
Minton D. A. (2008) The topographic limits of gravitationally bound, rotating sand piles. *Icarus, 195(2),* 698–704.
Mouret S., Hestroffer D., and Mignard F. (2007) Asteroid masses and improvement with Gaia. *Astron. Astrophys., 472,* 1017–1027.
Mueller M., Marchis F., Emery J. P., et al. (2010) Eclipsing binary Trojan asteroid Patroclus: Thermal inertia from Spitzer observations. *Icarus, 205,* 505–515.
Nolan M. C., Asphaug E., Greenberg R., and Melosh H. J. (2001) Impacts on asteroids: Fragmentation, regolith transport, and disruption. *Icarus, 153(1),* 1–15.
Ostro S. J., Scott R., Nolan M. C., et al. (2000) Radar observations of asteroid 216 Kleopatra. *Science, 288(5467),* 836–839.
Ostro S. J., Margot J. -L., Benner L. A. M., et al. (2006) Radar imaging of binary near-Earth asteroid (66391) 1999 KW4. *Science, 314,* 1276–1280.
Parker A., Ivezić Ž., Jurić M., et al. (2008) The size distributions of asteroid families in the SDSS Moving Object Catalog 4. *Icarus, 198,* 138–155.
Pätzold M., Andert T., Asmar S. W., et al. (2011) Asteroid 21 Lutetia: Low mass, high density. *Science, 334,* 491.
Poincaré H. (1885) Sur l'équilibre d'une masse fluide animée d'un mouvement de rotation. *Acta Mathemat., 7(1),* 259–380.
Polishook D., Moskovitz N., Binzel R. P., et al. (2014) Observations of fresh and weathered surfaces on asteroid pairs and their implications on the rotational-fission mechanism. *Icarus, 233,* 9–26.
Popova O., Borovička J., Hartmann W. K., et al. (2011) Very low strengths of interplanetary meteoroids and small asteroids. *Meteoritics & Planet. Sci., 46(10),* 1525–1550.
Pravec P. (2014) Asteroid spin-up fission systems. In *Asteroids, Comets, Meteors 2014, Book of Abstracts* (K. Muinonen et al., eds.), p. 451. University of Helsinki, Finland.
Pravec P., Vokrouhlickỳ D., Polishook D., et al. (2010) Formation of asteroid pairs by rotational fission. *Nature, 466(7310),* 1085–1088.
Pravec P., Scheirich P., Ďurech J., et al. (2014) The tumbling spin state of (99942) Apophis. *Icarus, 233,* 48–60.
Prockter L., Thomas P., Robinson M., et al. (2002) Surface expressions of structural features on eros. *Icarus, 155(1),* 75–93.
Ralchenko M., Britt D. T., Samson C. et al. (2014) Bulk physical properties of the Tagish Lake meteorite frozen pristine fragments. *Lunar Planet. Sci. XLV,* Abstract #1021. Lunar and Planetary Institute, Houston.
Richardson J. E. and Bowling T. J. (2014) Investigating the combined effects of shape, density, and rotation on small body surface slopes and erosion rates. *Icarus, 234,* 53–65.
Richardson D. C., Bottke W. F., Love S. G., et al. (1998) Tidal distortion and disruption of Earth-crossing asteroids. *Icarus, 134(1),* 47–76.
Richardson D. C., Leinhardt Z. M., Melosh H. J., et al. (2002) Gravitational aggregates: Evidence and evolution. In *Asteroids III* (W. F. Bottke Jr. et al., eds.), pp. 501–515. Univ. of Arizona, Tucson.
Richardson J. E., Melosh H. J., and Greenberg R. (2004) Impact-induced seismic activity on asteroid 433 Eros: A surface modification process. *Science, 306(5701),* 1526–1529.
Richardson D. C., Elankumaran P., and Sanderson R. E. (2005) Numerical experiments with rubble piles: Equilibrium shapes and spins. *Icarus, 173(2),* 349–361.
Robert O., Lognonne P., Scheeres D. J., et al. (2010) Seismology on a small body: Expected results for the BASiX Discovery mission proposal. Abstract U51B-0044 presented at 2010 Fall Meeting, AGU, San Francisco, California, 13–17 Dec.
Robinson M. S., Thomas P. C., Veverka J., et al. (2002) The geology of 433 Eros. *Meteoritics & Planet. Sci., 37(12),* 1651–1684.
Roche E. (1850) La figure dune masse fluide soumise lattraction dun point loign. *Acad. Sci. Montpellier,1,* 1847–1850.
Rozitis B., MacLennan E., and Emery J. P. (2014) Cohesive forces prevent the rotational breakup of rubble-pile asteroid (29075) 1950 DA. *Nature, 512(7513),* 174–176.
Russell C. T., Raymond C. A., Coradini A., et al. (2012) Dawn at Vesta: Testing the protoplanetary paradigm. *Science, 336,* 684–686.
Sánchez P. and Scheeres D. J. (2011) Simulating asteroid rubble piles with a self-gravitating soft-sphere distinct element method model. *Astrophys. J., 727,* 120.
Sánchez P. and Scheeres D. J. (2012) DEM simulation of rotation-induced reshaping and disruption of rubble-pile asteroids. *Icarus, 218,* 876–894.
Sánchez P. and Scheeres D. J. (2014) The strength of regolith and rubble pile asteroids. *Meteoritics & Planet. Sci., 49(5),* 788–811.
Scheeres D. J. (2002) Stability in the full two-body problem. *Cel. Mech. Dyn. Astron., 83(1),* 155–169.
Scheeres D. J. (2007) Rotational fission of contact binary asteroids. *Icarus, 189,* 370–385.
Scheeres D. J. (2009a) Minimum energy asteroid reconfigurations and catastrophic disruptions. *Planet. Space Sci., 57(2),* 154–164.
Scheeres D. J. (2009b) Stability of the planar full 2-body problem. *Cel. Mech. Dyn. Astron., 104(1),* 103–128.
Scheeres D. J. (2012) Minimum energy configurations in the n-body problem and the celestial mechanics of granular systems. *Cel. Mech. Dyn. Astron., 113(3),* 291–320.
Scheeres D. J. (2015) Landslides and mass shedding on spinning spheroidal asteroids. *Icarus, 247,* 1–17.
Scheeres D. J. and Gaskell R. W. (2008) Effect of density inhomogeneity on YORP: The case of Itokawa. *Icarus, 198(1),* 125–129.
Scheeres D. J., Khushalani B., and Werner R. A. (2000a) Estimating asteroid density distributions from shape and gravity information. *Planet. Space Sci., 48,* 965–971.
Scheeres D. J., Ostro S. J., Werner R. A., et al. (2000b) Effects of gravitational interactions on asteroid spin states. *Icarus, 147(1),* 106–118.
Scheeres D. J., Asphaug E. I., Colwell J., et al. (2003) Asteroid surface science with pods. *Lunar Planet. Sci. XXXIV,* Abstract #1444. Lunar and Planetary Institute, Houston.
Scheeres D. J., Benner L. A. M., Ostro S. J., et al. (2005) Abrupt alteration of asteroid 2004 MN4's spin state during its 2029 Earth flyby. *Icarus, 178(1),* 281–283.
Scheeres D. J., Fahnestock E. G., Ostro S. J., et al. (2006) dynamical configuration of binary near-Earth asteroid (66391) 1999 KW4. *Science, 314,* 1280–1283.

Scheeres D. J., Abe M., Yoshikawa M., et al. (2007) The effect of YORP on Itokawa. *Icarus 188,* 425–429.
Scheeres D. J., Hartzell C. M., Sánchez P., and Swift M. (2010) Scaling forces to asteroid surfaces: The role of cohesion. *Icarus, 210,* 968-984.
Scheirich P., Urech J. D., Pravec P., et al. (2010) The shape and rotation of asteroid 2008 TC3. *Meteoritics & Planet. Sci., 45(10–11),* 1804–1811.
Scheirich P., Pravec P., Jacobson S. A., et al. (2015) The binary near-Earth asteroid (175706) 1996 FG3 — an observational constraint on its orbital stability. *Icarus, 245,* 56–63.
Sharma I. (2013) Structural stability of rubble-pile asteroids. *Icarus, 223,* 367–382.
Sharma I., Burns J. A., and Hui C. -Y. (2005) Nutational damping times in solids of revolution. *Mon. Not. R. Astron. Soc., 359(1),* 79–92.
Sharma I., Jenkins J. T., and Burns J. A. (2009) Dynamical passage to approximate equilibrium shapes for spinning, gravitating rubble asteroids. *Icarus, 200(1),* 304–322.
Statler T. S. (2009) Extreme sensitivity of the YORP effect to small-scale topography. *Icarus, 202(2),* 502–513.
Tanga P., Comito C., Paolicchi P., et al. (2009) Rubble-pile reshaping reproduces overall asteroid shapes. *Astrophys. J. Lett., 706(1),* L197.
Takahashi Y. and Scheeres D. J. (2014) Morphology driven density distribution estimation for small bodies. *Icarus, 233,* 179–193.
Tedesco E. F., Williams J. G., Matson D. L., et al. (1989) Three-parameter asteroid taxonomy classifications. In *Asteroids II* (R. P. Binzel et al., eds.), pp. 1151–1161. Univ. of Arizona, Tucson.
Tholen D. J. and Barucci M. A. (1989) Asteroid taxonomy. In *Asteroids III* (R. P. Binzel et al., eds.), pp. 298–315. Univ. of Arizona, Tucson.
Thomas P. C. and Robinson M. S. (2005) Seismic resurfacing by a single impact on the asteroid 433 Eros. *Nature, 436,* 366–369.
Tsuchiyama A., Uesugi M., Matsushima T., et al. (2011) Three-dimensional structure of Hayabusa samples: Origin and evolution of Itokawa regolith. *Science, 333(6046),* 1125–1128.
Tsuda Y., Yoshikawa M., Abe M., Minamino H., and Nakazawa S. (2013) System design of the Hayabusa 2 asteroid sample return mission to 1999 JU3. *Acta Astronaut., 91,* 356–362.
Urakawa S., Ohtsuka K., Abe S., Ito T., and Nakamura T. (2014) Fast rotation of a subkilometer-sized near-Earth object 2011 XA3. *Astron. J., 147(5),* 121.
Vokrouhlickỳ D. and Nesvornỳ D. (2008) Pairs of asteroids probably of a common origin. *Astron. J., 136(1),* 280.
Vokrouhlickỳ D., Breiter S., Nesvornỳ D., and Bottke W. F. (2007) Generalized YORP evolution: Onset of tumbling and new asymptotic states. *Icarus, 191(2),* 636–650.
Walsh K. J. and Richardson D. C. (2006) Binary near-Earth asteroid formation: Rubble pile model of tidal disruptions. *Icarus, 180(1),* 201–216.
Walsh K. J., Richardson D. C., and Michel P. (2008) Rotational breakup as the origin of small binary asteroids. *Nature, 454(7201),* 188–191.
Walsh K. J., Richardson D. C., and Michel P. (2012) Spinup of rubble-pile asteroids: Disruption, satellite formation, and equilibrium shapes. *Icarus, 220(2),* 514–529.
Warner B. D., Harris A. W., and Pravec P. (2009) The asteroid lightcurve database. *Icarus, 202(1),* 134–146.
Washabaugh P. D. and Scheeres D. J. (2002) Energy and stress distributions in ellipsoids. *Icarus, 159(2),* 314–321.
Yano H., Kubota T., Miyamoto H., et al. (2006) Touchdown of the Hayabusa spacecraft at the Muses Sea on Itokawa. *Science, 312(5778),* 1350–1353.
Yeomans D. K., Antreasian P. G., Barriot J.-P., et al. (2000) Radio science results during the NEAR-Shoemaker spacecraft rendezvous with Eros. *Science, 289,* 2085–2088.